Nanoscale

REVIEW

View Article Online
View Journal | View Issue

Cite this: *Nanoscale*, 2025, **17**, 25975

Microwave chemistry and microwave-assisted synthesis of nanomaterials in biomedicine: a focused review

Ankur Sood, [a,b] Kanika,[c] Arpita Roy, [d] Shubham Mahajan,[c] Sung Soo Han, [a,b] Rehan Khan *[c] and Sumanta Sahoo *[a]

The relentless surge in the demand for novel materials has driven the development of innovative fabrication methodologies that are motivated by minimized energy utilization and sustainable chemical processing as researchers are increasingly compelled to adopt more environmentally benign fabrication methods. To align with the principles of green chemistry, microwave-assisted synthesis (MAS) has been marked as one of the well-established technologies in various research fields. This review emphasizes on the MAS of nanomaterials (NMs) while concentrating on its biomedical applications. In this perspective, we delve into the basis of the MAS of NMs while highlighting the mechanism of heating involved in MAS. Compared with the existing reviews in this field, this review aims to offer a comprehensive analysis of the regulatory parameters, such as the choice of solvent, frequency, power, and irradiation time in designing the MAS of NMs. This review argues for a multidimensional property assessment on the selection of NMs and MAS-linked parameters to establish the targeted biomedical applications, such as cancer therapy, drug delivery, and tissue engineering (2019–2025), which is unique to this review compared with the existing ones. Finally, this review spotlights some key factors to be considered to increase the yield, purity, and efficiency of NMs fabricated *via* MAS. This perspective is aimed at offering a critical analysis of MAS and its utilization to supplement the synthesis of green and sustainable materials.

Received 25th August 2025,
Accepted 18th October 2025

DOI: 10.1039/d5nr03588k

rsc.li/nanoscale

1. Introduction

Advances in materials sciences, exemplified by the fabrication of diverse nanostructures, hold immense potential in every stretch of science and technology.[1,2] Nanomaterials (NMs) have demonstrated great potential in the biomedical field due to their exceptional physicochemical properties, like fluorescence, adhesion, and photothermal, optical, electrical, and mechanical properties, compared with their macroscale counterparts.[3] When materials are reduced to the nanoscale, they undergo substantial structural and functional changes, precisely guiding their interaction with cells and biomolecules. NMs could modulate the cellular structure, initiate cell–cell interactions, induce or prevent cell adhesion and aggregation, and intervene in deciding the cell fate.[4,5]

The progress in the fabrication of NMs is destined to embrace innovative approaches and synthesis routes, epitomized by the manufacturing of NMs of distinct shapes and sizes. NMs and nanostructures (NSs), due to their unique properties, including a high surface-to-volume ratio, biocompatibility, and tunable surface properties, facilitate interaction with biological systems and show potential in target therapy and drug delivery systems, making them potent candidates for biomedical applications.[6–9] The realm of NM fabrication has embraced several conventional top-down/bottom-up approaches, many of which are associated with environmental concerns.[10,11] Currently, substantial efforts are dedicated to minimize the energy utilization and achieve sustainable chemical processing as researchers are persistently confronted to adopt more environmentally benign fabrication methods.[12–14] In order to align with the principles of green chemistry, microwave (MW)-assisted synthesis (MAS) has been marked as one of the breakthrough technologies with propitious future prospects.[15–20] MAS involves the utilization of MWs, which are electromagnetic waves consisting of both electric and magnetic components.[21] In the MAS process, when a

[a]*School of Chemical Engineering, Yeungnam University, 280 Daehak-ro, Gyeongsan 38541, South Korea. E-mail: sumanta95@gmail.com*
[b]*Institute of Cell Culture, Yeungnam University, 280 Daehak-ro, Gyeongsan 38541, South Korea*
[c]*Chemical Biology Unit, Institute of Nano Science and Technology, Knowledge City, Sector 81, Mohali (SAS Nagar) 140306, Punjab, India. E-mail: rehankhan@inst.ac.in*
[d]*Department of Chemical and Biomolecular Engineering, University of California Los Angles, Los Angeles, CA, 90095, USA*

material is exposed to MWs, the ion field or dipoles on the material attempt to align with the oscillating electric field. During this process, as a result of molecular frictions and dielectric losses, energy is lost in the form of heat.[22–24] MAS could be executed in reaction vials that are transparent to electromagnetic waves, and thus the MWs can easily pass through the walls of the reaction vial, thereby interacting directly with the ions in the reaction mixture.[25,26] This reduces the tendency for the reaction mixture to boil and results in high purity and crystal growth. Compared to the conventional synthetic routes such as hydrothermal, solvothermal, and wet chemical synthesis, the widespread acceptability and credibility of MAS are attributed to several factors, including its facile and rapid synthetic route with enhanced reaction rate, uniform heat distribution, minimal environmental impact, reproducibility, higher energy efficiency, and large scaling-up potential.[16,18,27–29] In recent times, MAS approaches have been significantly investigated for various applications, including biomedical applications.[30–41] However, very few review articles have been dedicated this topic in the last few years.[19,42–46] Thus, considering the huge potential of MAS approaches, a timely, comprehensive review article is highly essential.

This review provides a comprehensive analysis of the MAS-based fabrication of NMs and their utility in biomedical applications such as cancer therapy, drug delivery, and tissue engineering (2019–2025). This review highlights the progress in MAS and critically discusses the mechanism of heating and the parameters regulating the process of MAS. Furthermore, it details the basics of NMs and their fabrication using MAS, along with the parameters associated with MAS (effect of solvent, irradiation time, and heating power) that could affect the size, shape, and properties of NMs and NSs. The discussion emphasizes the criteria of solvent selection, MW parameters, and materials that could affect the size, morphology, functionality, and architecture of NMs and NSs, which could be directly linked to their performance in biomedical applications. Additionally, it explores various applications of NMs fabricated using MAS in the field of biomedicine. By integrating the latest expansions and exploring detailed functionalities, this review aims to be a timely, comprehensive, and critical resource for researchers, thus assisting the ongoing innovations in the field of MAS.

This review comprises 4 sections. The first section gives a brief overview of the importance of MAS and its utility in the synthesis of NMs, while highlighting its advantage over other synthetic routes. In section 2, a comprehensive overview of MAS is demonstrated, which encompasses the basics of MWs, the underlying mechanism of heating with MWs, and the regulatory parameters affecting the yield in the MAS of NMs. Section 3 presents the recent advancements in the MAS-based synthesis of NMs, while differentiating the different categories of NMs fabricated thus far using MAS. Section 4 covers the applications of the fabricated NMs using MAS in the field of tissue engineering, cancer therapy, and biosensing to date. This review concludes with a critical evaluation of the current challenges in the MAS-based fabrication of NMs, which include selection of MW parameters, scale-up strategies, and selection of appropriate materials, and addresses these challenges for future prospects. The current review article demonstrates a strong correlation among materials science, physics, and biomedical engineering, which will be highly beneficial for readers. A schematic illustration of content in this review is presented in Fig. 1.

2. Microwave-assisted synthesis (MAS)

Electromagnetic (EM) wave radiation has been significantly utilized for the development of nanostructured materials because of its rapid heating approach, as well as contactless synthetic protocols.[20] Electromagnetic radiation includes radiation of different frequencies, including X-rays, MW, IR, UV-visible, radio waves, and γ-rays. Among them, the utilization of MW irradiation (MWI) to accelerate the reaction rate has emerged as a promising strategy for synthesizing both inorganic and organic materials.[13,47,48]

2.1. Basics of microwave irradiation

MWI can be classified as EM radiation in the frequency range of 0.3–300 GHz, corresponding to the wavelength range of 1 mm–1 m. In the EM wave spectrum, MWs are between the IR and radio wave range. However, domestic MW ovens operate at a frequency of 2.45 GHz, corresponding to the wavelength of 12.2 cm. It is important to note that the energy of MWs is insufficient for breaking chemical bonds. Accordingly, MW-assisted synthetic approaches are based on the efficient heating of materials. Unlike photochemical reactions, no chemical reaction occurs through the absorption of MW radiation. Both solid-state and liquid-phase MW-assisted approaches have been reported for the effective synthesis of nanostructured materials for various applications, including energy storage/conversion, environmental remediation, and bio-medical applications,[28,49–52] The advantages of MAS approaches are listed below.

(a) Fast reaction rate. The utilization of MWI significantly reduces the reaction time from several hours to a few minutes or even a few seconds. The fast heating process not only decreases the reaction time for the organic compounds but is also found to be effective for the synthesis of metal and metal oxide nanoparticles (NPs).

(b) High product yield with high purity. Because of the rapid heating process, there is less possibility of the formation of side products through MAS processes. Therefore, compared to the conventional chemical reaction processes, MAS approaches result in the production of a higher quantity of NMs with high purity.

(c) Green synthetic route. In the current scenario, where achieving a green and sustainable future is highly essential, MAS approaches are indispensable. Specifically, solid-state MAS approaches do not utilize any solvents, indicating a clean, environment-friendly synthetic protocol. Moreover, the lack of purification steps in MAS approaches also reduces the involvement of toxic reagents.

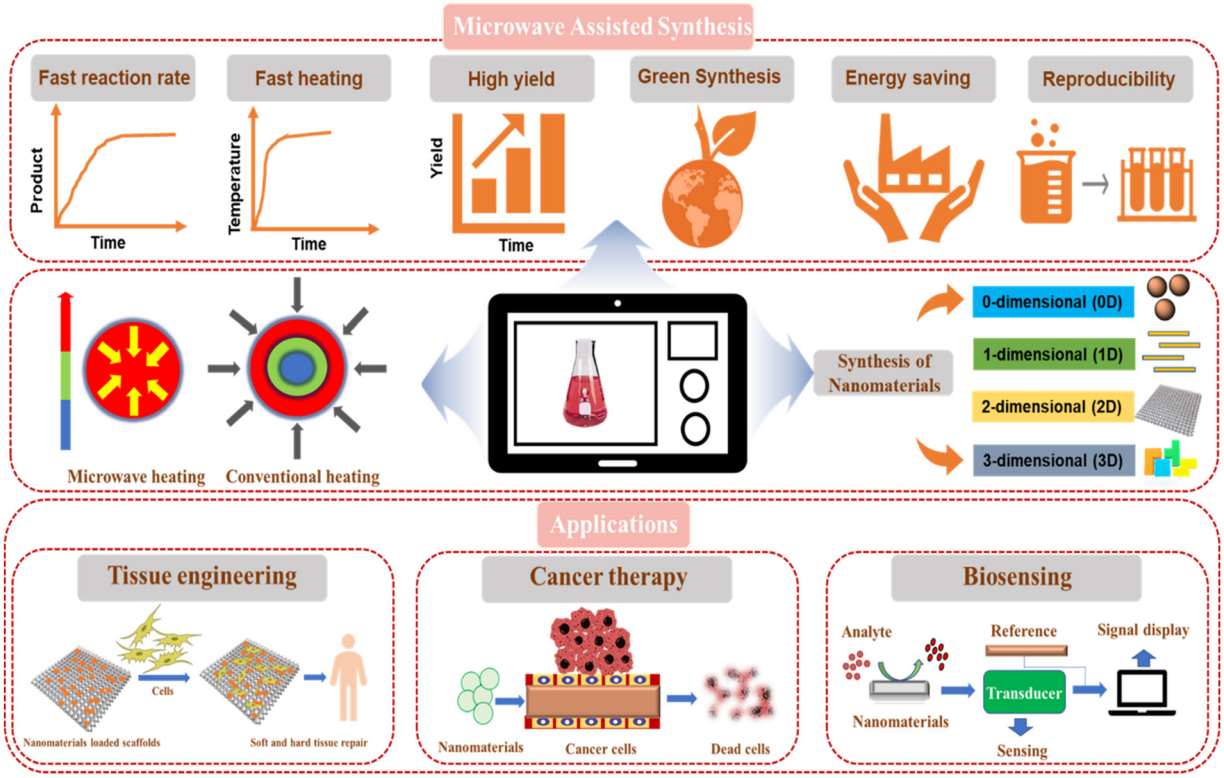

Fig. 1 Overview of this review, including the basis of MW-assisted synthesis and its advantages and applications in biomedicine.

(d) Energy-saving approach. The MAS approach can be considered efficient and energy-saving in terms of its shorter reaction time and selective heating system. Moreover, unlike the conventional approaches, MWI only heats the material, not the reaction container or apparatus, indicating lower energy consumption.

(e) High reproducibility. The uniform heating system in the MAS approach induces high reproducibility, which is also beneficial in comparison to the conventional approaches.

2.2. Mechanism of heating

The mechanism of MW heating is different from the conventional heating process. Although conventional heating synthesis (CHS) follows the thermal conduction mechanism, liquid-phase MAS approaches generally follow two types of mechanisms, *i.e.*, the dipolar polarization mechanism and the ionic conduction mechanism.[52,53] In the dipolar mechanism, heat is generally produced through the collision between polar molecules. At a particular frequency, the polar molecules tend to orient themselves with the electromagnetic field, which results in random motion, initiating resonance and oscillation, and eventually producing heat. Conversely, in the conduction mechanism, heat generation is caused by the collision of dissolved ions and electrons under the influence of a MW field. In the case of solid-state MAS approaches, the heating process follows an interfacial polarization mechanism, which can be considered the combination of the two above-mentioned mechanisms of MW heating.[54–56]

Unlike CHS, in MAS approaches, the heating process is simultaneous and starts from the surface to the bulk of the target material. Furthermore, the heating process is contactless, which refers to the non-requirement of physical contact between the surface of the material and the reaction container. Additionally, the slow heating process in CHS significantly affects large-scale production, whereas MAS approaches are highly advantageous for commercial use due to their fast heating process. In this aspect, a previous report compared the effect of MW heating and conventional heating on the properties of activated carbon (AC) synthesized from a biomass precursor, *i.e.*, *Jatropha* hull.[57] It was evident that the AC synthesized through CHS demonstrated a surface area of 748 $m^2\ g^{-1}$, whereas the AC synthesized through MAS achieved a surface area of 1350 $m^2\ g^{-1}$ with a lower pore size. In another work, the utilization of MAS reduced the processing time for the extraction of pectin from dragon fruit and passion fruit peels.[58] These MAS processes have a significant impact on the synthesis of metal NPs. For example, in a previous report, Dahal *et al.* demonstrated that the utilization of MW heating enhanced the crystallinity, monodispersity, and also control over the morphology of Rh, Pd, and Pt NPs.[59] In another work, a MW furnace demonstrated 4 times lower processing time and 5 times lower energy consumption compared to conventional furnaces for the synthesis of $NaAlH_4$.[60]

Controversies regarding non-thermal MW effects: Dipolar rotation and ionic conduction are believed to be the primary mechanisms *via* which MWs exert thermal effects, consequently enhancing the reaction rate. However, there is an ongoing debate as to whether these effects, standing alone, can drastically catalyze MAS reactions, or there are certain non-thermal effects that may also be prominently responsible for this phenomenon. Recent research by Wang *et al.* focused on the role of non-thermal aspects of MAS, and it was observed that the MW field apparently alters the reaction mechanisms *via* ways such as field-induced excitation and selective molecular excitation. These studies indicate the underlying role of non-thermal effects of MWs in accelerating reactions.[61] However, contradicting observations by De la Hoz *et al.* and Moreno *et al.* paint a different portrait, where the authors state that non-thermal MW effects might be minimal in liquid-phase reactions due to the rapid redistribution of energy, and may be confused with local superheating, erratic temperatures, and flawed protocol design and experimental setup.[62,63] Researchers also agree that non-thermal effects are difficult to quantify and require sophisticated instrumentation such as fiber-optic thermometry and *in situ* spectroscopy for detection and analysis.

Therefore, non-thermal effects of MW may be an understated player in hastening MAS reactions, and further research is warranted for establishing this. Especially in the case of heterogeneous or confined reaction systems, an increase in dipole alignment, interface-aimed electric fields, and preferred energy absorption at polar intermediates indicates non-thermal effects. These non-thermal effects may enhance the plasma generation and diffusion rates in solid particles. Therefore, research on these non-thermal effects may be necessary for fully understanding the reaction mechanisms catalyzing and altering chemical reactions in MAS.

2.3. Parameters regulating microwave synthesis

The MAS approach not only enhances the nucleation rate but also effectively influences the characteristics of nanostructured materials. However, several parameters influence this approach, and depending on these parameters, the properties of the synthesized materials vary. The effects of these parameters are summarized below.

(a) Effect of solvent. The solvents play a significant role in MAS processes. The capacity of a solvent for the conversion of EM energy to thermal energy at a constant frequency is known as the loss tangent ($\tan\delta$), which is calculated by dividing the dielectric loss by the dielectric constant. A solvent with a high loss tangent value ($\tan\delta > 0.5$) is considered a good MW absorber, and therefore it offers an efficient heating process. Conversely, solvents with a loss tangent value of 0.1–0.5 are designated as medium MW absorbers. However, solvents with a loss tangent value of <0 are poor MW absorbers.[64] In this case, ethylene glycol is considered a good solvent in MAS approaches with a $\tan\delta$ value of 1.350 and water is considered a medium MW absorber with a loss tangent value of 0.123.[65] However, water is considered a promising solvent in MAS approaches for synthesizing organic molecules because of its low cost and non-toxic nature. The effect of various solvents on the morphology has been clearly observed for the synthesis of ZnO NPs, as shown in Fig. 2(a–d).[66] The usage of ethylene glycol and digol as the solvents resulted in the formation of a hexagonal prism-like structure. However, in the presence of water, hexagonal plate-like structures were formed. Conversely, the usage of 2-propanol resulted in the formation of agglomeration.

(b) Effect of MW power. The size and shape of NMs vary with a variation in MW power. In this aspect, a previous report demonstrated the effect of MW power on the synthesis of Au NPs.[67] It is evident that the nucleation dynamics of the synthesis of Au NPs can be modulated by adjusting the MW power. The utilization of higher MW power at an early stage resulted in the formation of uniform NPs with a reduced size. Also, a change in MW power significantly affects the morphology of metal NPs. In this context, Yang *et al.* showed that adjusting the MW power between 10 and 800 W can dramatically change the length and shape of silver nanowires.[68] Low power leads to short wires and some nanorods, while moderate power (around 320 W) strikes a balance-slowing the reduction just enough to allow the formation of longer, more consistent nanowires. However, when the power is too high, the reaction speeds up too much, disrupting seed formation and causing shorter wires and larger particles to appear instead.

Apart from metals, variations in the morphologies of metal oxide nanostructures have also been observed with a change in the MW power. Increased MW power significantly affects the properties of ZnO nanostructures. Increasing the power from 150 to 1000 W (for 5 min) increases the average crystallite size.[69] Significant morphological changes have also been observed with changes in MW power. At low MW power (150 W), the polarization and aggregation of ZnO nuclei resulted in the formation of ZnO NPs, whereas at higher power (450 W, 700 W, and 1000 W), nanoneedles and nanosheets of ZnO were formed because of the presence of additional growth units and a fast growth rate. Apart from these morphological changes, the MW power also significantly affects the crystallinity of metal oxide nanostructures. As reported by Promnopas *et al.*, an enhancement in MW power from 400 to 800 W resulted in an increased particle size and crystallinity of ZnO crystals.[70] The increment in MW power resulted in a narrower energy band gap with the decrease in the FWHM of the characteristic (101) peaks in the XRD patterns (Fig. 2(e and f), respectively). In another work, a change in MW power from 540 to 680 encouraged the synthesis of flower-shaped ZnO NPs.[71] Overall, it can be concluded that the MW power has a noteworthy effect on the morphology, size, crystallinity, *etc.* of metal/metal oxide nanostructures.

(c) Effect of MW frequency. The MW frequency plays a significant role in the nucleation and growth of NMs. In this aspect, Ashley *et al.* demonstrated the effect of MW frequency on the growth of Ni nanocrystals from Ni salt precursor using a mild reducing agent.[72] For a constant reaction time, increasing the frequency from 2.45 GHz to 15.50 GHz reduced the

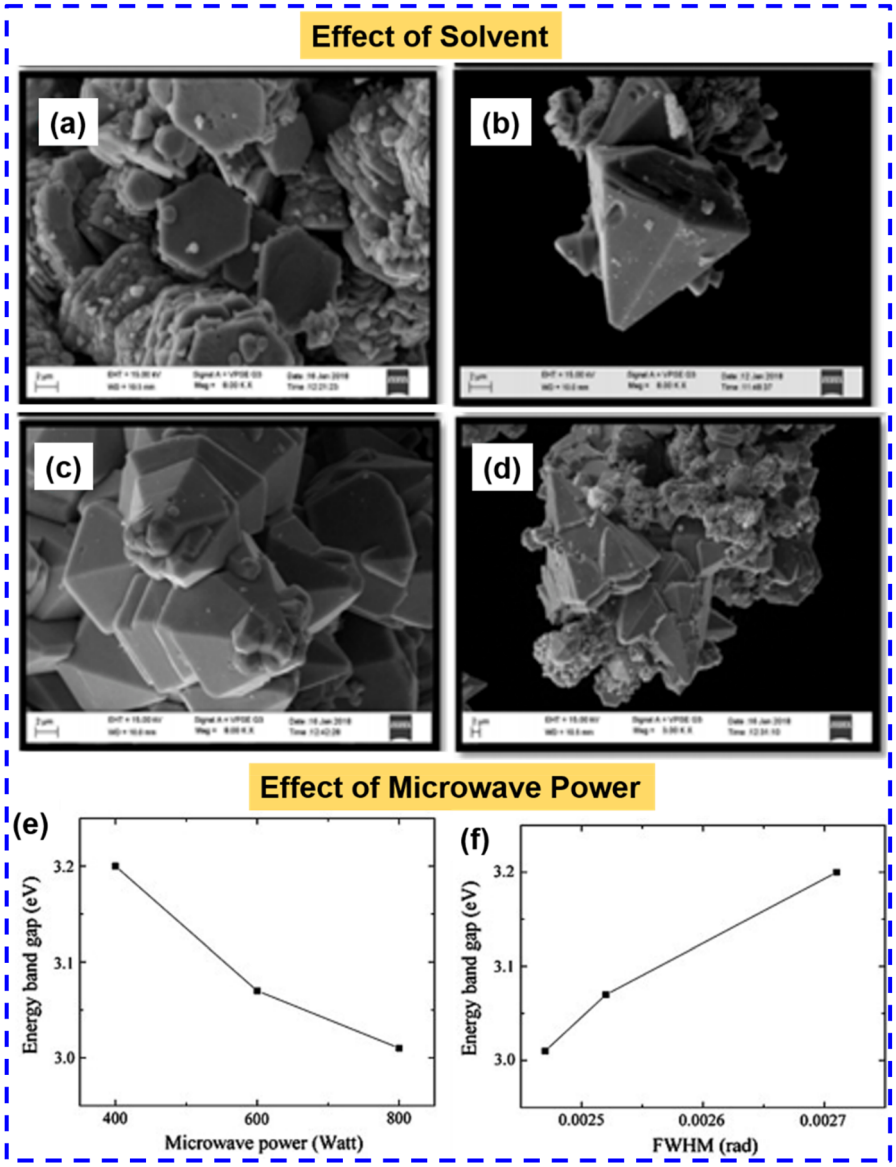

Fig. 2 Effect of solvent: SEM images of ZnO NPs synthesized through the MAS approach using different solvents: (a) water, (b) ethylene glycol, (c) digol, and (d) 2-propanol.[66] Effect of MW power (e) and (f) FWHM on the energy gap of ZnO NPs.[68] (a–d) Reproduced from ref. 66, with permission from Elsevier, Copyright 2020. (e and f) Reproduced with permission from ref. 68 with permission from Elsevier, Copyright 2011.

average NP diameter from 35.1 nm to 18.8 nm. However, a further increase to 18 GHz resulted in a slight increase in size to 21.2 nm. This non-linear behavior highlights how changes in frequency alter the underlying nucleation and growth kinetics. In another work, Horikoshi *et al.* investigated the effect of MW frequency on the formation of Au NPs in both polar and non-polar solvents.[73] Interestingly, the increment in MW frequency from 2.45 to 5.8 GHz did not show any effect on the size and shape of the Au NPs in a polar solvent (polyvinylpyrrolidone). In contrast, when a nonpolar solvent was used, Au NPs were not formed at 2.45 GHz due to less MW absorption, while 6 nm Au NPs were observed at the frequency of 5.8 GHz.[73] The underlying cause of the non-formation of Au NPs at lower frequency could be insufficient heating, given that five-fold greater temperature was observed at the higher frequency. This heating difference is related to the dielectric properties of the medium. In the case of materials such as TiO_2 in an aqueous medium, the penetration depth of MWs is strongly dependent on the frequency. Lower frequencies, such as 2.45 GHz, penetrate much deeper (up to 4.8 cm at 99 °C) (Fig. 3(a)), whereas higher frequencies, such as 5.8 GHz, penetrate much shallower (up to 0.62 cm). Despite this, higher frequencies often show a dominating, faster heating characteristic, as observed in the TiO_2 system (Fig. 3(b)).[74] A previous article demonstrated the MW-assisted hydrothermal synthesis of $BaTiO_3$ nanocrystals.[75] In this process, an increase in frequency from 2.45 GHz to 4 GHz dramatically increased the surface area from 12 $m^2\ g^{-1}$ to 37 $m^2\ g^{-1}$. Furthermore, the

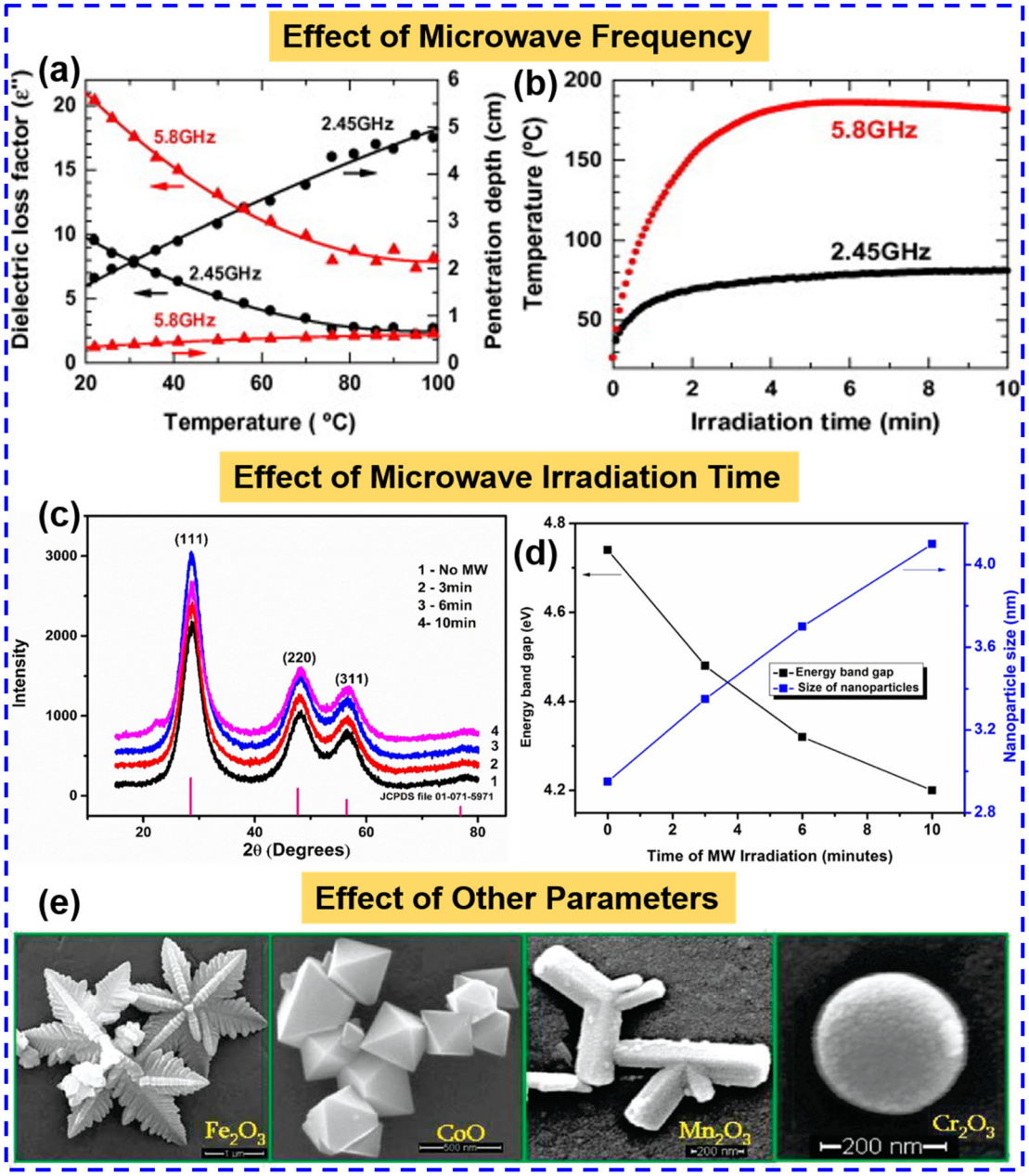

Fig. 3 Effect of MW frequency: (a) temperature profiles for the variations in the dielectric loss factor and the penetration depth of the 2.45 GHz and 5.8 GHz MWs into water and (b) temperature–irradiation time profiles resulted from the absorption of 2.45 GHz and 5.8 GHz MW radiations by the powdered TiO_2 systems.[74] Effect of MW irradiation time: (c) XRD patterns of ZnS synthesized through MW irradiation for different time intervals and (d) influence of MW irradiation time on the size and energy bad gap of ZnS NPs.[80] Effect of other parameters: (e) change in morphology of Fe_2O_3, CoO, Mn_2O_3, and Cr_2O_3 upon the substrate concentration variations and reaction temperature in MW-assisted hydrothermal approach.[87] (a and b) Reproduced from ref. 74 with permission from The Royal Society of Chemistry, Copyright 2011, (c and d) reproduced with permission from ref. 80 with permission from Elsevier, Copyright 2022, (e) reproduced with permission from ref. 87 with permission from the American Chemical Society, Copyright 2009.

shape of the particles shifted from cubic to spherical when the frequency reached 5.5 GHz, again pointing to a fundamental change in the crystallization process driven by the MW frequency. Apart from these reports, the effect of MW frequency on surface morphology, size, and shape has further been monitored for CdS NPs,[76] iron oxide NPs,[77] and TiO_2 NPs.[78]

(d) Effect of MW irradiation time. In MAS approaches, the MW irradiation time has a substantial impact on the reaction rate. In a previous study, it was observed that an increment in MW irradiation time from 5 to 10 min enhanced the uniformity in the morphology of ZnO nanosheets.[69] In another work, Barreto *et al.* demonstrated that an increment in MW

irradiation time subsequently improves the homogeneity of the particle size and morphology of ZnO NPs.[79] Furthermore, an enhancement in MW irradiation time from 3 to 10 min enhanced the size of ZnS NPs from 3.35 to 4.1 nm.[80] As shown in Fig. 3(c), the XRD patterns of ZnS NPs synthesized at different MW exposure times indicate the increment in crystallinity with an increase in MW irradiation time. Moreover, lowering of the band gap and an increment in particle size have also been observed in ZnS NPs with an increase in MW irradiation time, as shown in Fig. 3(d). Furthermore, more exposure to MW further enhanced the polycrystallinity of these metal sulfide NPs. This an increment in particle size with an increment in MW irradiation time was further observed for CuSe NPs.[81] In this work, the CuSe NPs synthesized at a constant MW power of 380 W for the MW irradiation time of 10 min displayed an optical band gap of 1.85 eV. However, their optical band gap was reduced to 1.60 eV with an increment in MW irradiation time to 30 min, indicating an increase in crystallite size. Herein, the MW exposure for a longer time enabled more particles to fuse together to enhance the size of the particles through the Ostwald ripening process. This tuning in size with a change in MW irradiation time has further been observed for Ag NPs,[82,83] Au NPs,[84,85] and PbS NPs.[86]

(e) Effect of other parameters. Apart from the above-mentioned parameters, some other factors affect the growth and characteristics of nanostructured materials synthesized through MAS approaches. For example, the pH of the precursor solution displayed a significant impact on the uniformity of Au NPs.[67] pH $\geq$ 6.2 is suitable for synthesizing less reactive Au solute complexes, which led to a stable reaction and influenced the formation of a uniform colloidal solution of Au NPs. Similar to other conventional approaches, the change in the precursor significantly affected the morphology of the end-product in MAS approaches. It was evident that the particle size of MAS-synthesized ZnO decreased with a change in precursor anions from NO_3^- to CH_3COO^- to Cl^-.[79] In another work, Polshettiwar *et al.* demonstrated the tailoring of the size and shape of various nanostructured metal oxides by varying the substrate concentration and the reaction temperature of the MW-assisted hydrothermal approach.[87] Through the self-assembly process, the adopted approach was able to synthesize nanostructured metal (Fe, Co, Mn, Cr, and Mo)-based oxides of various structures, including octahedron, pine, hexagonal snowflake, and triangular rod-like structures, as shown in Fig. 3(e). In another report, the addition of a surfactant resulted in the finer growth of particles through the MAS approach because of the capping effect.[88]

3. Microwave-assisted synthesis of different nanostructures

3.1. Nanomaterials and their composition-based classification

NMs as well as nanostructures (NSs) are rapidly advancing in research and commercial applications owing to their tuneable properties, including catalytic activity, scattering, wettability, thermal conductivity, and mechanical features.[89–92] NMs are typically defined as materials with one dimension ranging from 1 to 100 nm, though some classifications extend up to 1000 nm. The EU Commission defines NMs as natural or synthetic substances with unbound, aggregated, or agglomerated particles, featuring dimensions between 1 and 100 nm.[93] NMs are classified based on their morphology, including structure, size, and form. The classification of NMs has been exhibited in many criteria, including shape, size, and dimensions, but based on their composition and inter-component interactions, NMs are classified as of organic, inorganic, carbon-based, and hybrid NPs[94] (Fig. 4).

Organic NPs are signposted as a reflection of organic compounds at the nanoscale and comprise micelles, dendrimers, liposomes, nanogels, polymeric NPs, and multilayer biopolymers.[95] Micelles and liposomes, characterized by hollow, biodegradable, nontoxic structures, are reported to demonstrate sensitivity towards light, electromagnetic radiation, and heat,[96] whereas dendrimers are depicted to carry biomolecules or pharmaceutical agents in their internal holes and show target specificity due to the numerous chains decorating their surface, making them potent candidates for optoelectrochemical, sensing, and theranostic applications.[97–99] Moreover, nanogels, with their immense water-holding capacity, degradability, amphiphilicity, and porosity, play a vital role in tissue engineering and theranostic applications.[100] Additionally, polymeric NPs, also referred to as organic NPs, are used for protecting biomolecules from the surrounding environment, while increasing their bioavailability and therapeutic index.[101] Polymeric NPs include both nanocapsules and nanospheres, and have been explored for numerous healthcare applications, specifically in designing advanced drug delivery systems.[102] Nanospheres are comprised of a polymeric network in which drugs are retained or adsorbed on the NP surface, whereas in the case of nanocapsules, their oily core comprises the drug in a dissolved state, followed by a protective polymeric shell on the outer surface that regulates the drug release behaviour.[103] Additionally, nanocapsules comprised of many polymeric shells are also being fabricated, where the retention of biologically active molecules or drugs is higher, which in turn increases the regulated bioavailability of these drugs/molecules.

Inorganic NPs, lacking carbon, are hydrophilic in nature, non-toxic, and biocompatible with living systems, while being more stable compared to organic NPs.[104] Further, inorganic NPs demonstrate ease of surface functionalization, reduced side effects, high chemical stability, and cost-effective production, which make them a potent choice in many biomedical applications.[105] Compared to organic NPs, inorganic NPs have a high drug loading capacity, besides tunable degradation rate, making them a potential contender in various biomedical applications concerning drug delivery, imaging, and biosensing.[106,107] Some highly explored inorganic NPs include magnetic,[108,109] noble metal (Au, Ag, and Pt),[110–112] and transition metal (Fe, Co, Ni, Zr, and Hf) oxides.[113,114]

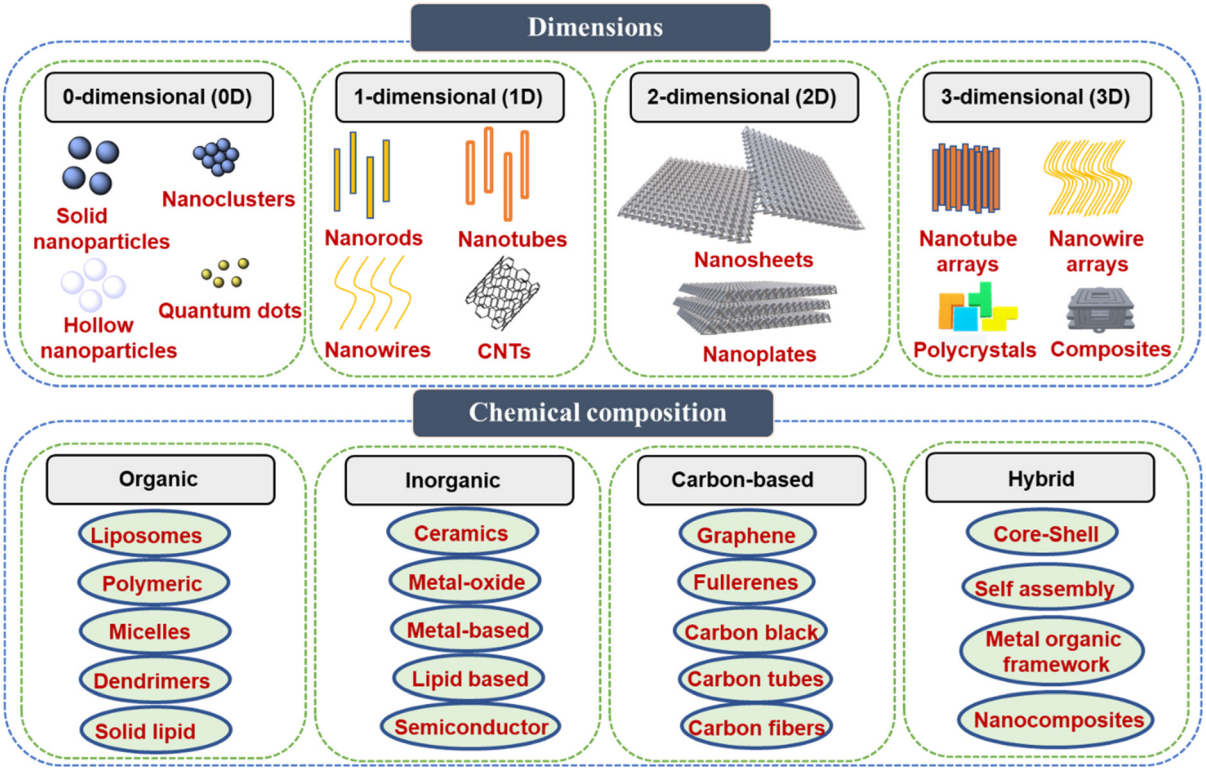

Fig. 4 Classification of NMs based on their dimensions and chemical compositions.

Magnetic NPs (mNPs), particularly iron oxide mNPs, are key inorganic NPs.[115] They aid in iron digestion and replenishment in the body, addressing its low bioavailability in biological tissues.[116] Cationic mNPs localize in endosomes for extended periods, enhancing their functional efficacy. Alternatively, metallic NPs are synthesized specifically from metals using either constructive or destructive methods, requiring metal precursors for purity. The unique properties of metallic NPs have paved their way for their advancement to the forefront of advanced science and technology applications. The fabrication of metallic NPs is not trivial and demands a deep understanding of the governing parameters and the composition chemistry of their precursors. Common examples include NPs of cadmium, aluminium, copper, silver, lead, cobalt, zinc, gold, and iron.[117,118] Moreover, noble metal NPs (Au, Pt, and Ag) are widely utilized in biomedical applications, including cancer therapy, diagnostics, radiation enhancement, antimicrobial control, thermal ablation, drug delivery, and gene transport. Their unique properties and higher functionality allow surface functionalization with antibodies, peptides, DNA, RNA, or biocompatible polymers such as polyethylene glycol to target diverse cell types.[119] On the contrary, metal oxide NPs have gained a critical place in modern technological advancements due to their facile fabrication approach and cost-effective synthetic routes with high yields. These metal oxide NPs are engineered to enhance their properties, exhibiting greater reactivity than their metal counterparts. Iron oxide NPs, in particular, have shown high reactivity and various applications in biomedical research, including significant antibacterial activity and enhanced imaging performance.[120–122] Besides, many metal oxide NPs have been explored in different frontiers of science and technology. For example, silver oxide (Ag_2O) NPs have been identified as a potential antibacterial source by many researchers.[123–125] In addition to Ag_2O NPs, the antibacterial effect has also been highlighted for many other metal oxide NPs. In this regard, Azam *et al.* studied the antibacterial effects of ZnO, Fe_2O_3, and CuO NPs against Gram-negative (*P. aeruginosa* and *E. coli*) and Gram-positive (*B. subtilis* and *S. aureus*) bacteria.[126]

Furthermore, to closely monitor the interaction of NMs and NSs in biological systems, the concept of bionanomaterials has emerged, which are atomic or molecular assemblies formed *via* biomolecules or NMs being encapsulated inside biomolecules.[127] Bionanomaterials are naturally occurring NPs with extracellular or intracellular structures, for example, exosomes, magnetosomes, lipoproteins, viruses, and ferritin. Magnetosomes are intracellular, while viruses and lipoproteins are extracellular structures.[128] In addition, carbon-based materials are valued for their diverse allotropes, including amorphous carbon, diamond, graphite, graphene quantum dots (GQDs), fullerene, graphene oxide (GO), and carbon nanotubes. Amorphous carbon is common, and carbon nanotubes are categorized into single-walled (SWCNTs) and multi-walled (MWCNTs) types.[129] Graphene quantum dots, a recent carbon-based biomaterial, have lateral dimensions under 100 nm, consist of a single or a few layers, and are considered zero-

dimensional graphene sheets. Graphene quantum dots, with accessible electrons and a large surface area, are ideal for biological applications such as biomolecule detection, cancer therapy, imaging, and targeted drug delivery, demonstrating effectiveness across various uses.[130] Carbon-based NPs are entirely composed of carbon and include carbon nanotubes, graphene, carbon nanofibers, fullerenes, and carbon black.[131]

The MAS of individual materials such as metallic NPs, metal oxides, and carbon-based nanostructures, such as covalent organic frameworks (COFs), graphene NPs, and nanotubes, has been explored in recent times due to the various aforementioned advantages of MAS compared to conventional methods. The major variation in their synthesis comprises MW power and frequency, choice of solvent/solvent-free approach, apparatus, and temperature.

3.2. Microwave-assisted synthesis of nanoparticles

MW-assisted synthesis has emerged as a prominent technique due to its ability to significantly reduce reaction times. Optimized methods enable the production of metal and metal oxide NPs with high yield and purity. Additionally, this method offers ease of scalability, making it advantageous for large-scale applications. The green synthesis of metal and metal oxide NPs has gained significant attention in recent years, particularly using MW-assisted techniques. Typically, nitrate or chloride salts serve as precursors, while plant extracts, polyphenols, probiotic broths, or natural polymers act as both stabilizers and reducing agents. The reduction of metal salts is often indicated by a visible colour change, signifying NP formation, which is subsequently confirmed using UV-Vis spectrometry. These NPs are further evaluated for biomedical applications, including antioxidant, antimicrobial, and anticancer activities, through various analytical assays.

NPs of noble metals such as silver (Ag NPs), gold (Au NPs), and platinum (Pt NPs) have been synthesized *via* MW-assisted green synthesis. For example, Ag NPs were synthesized using *Melia azedarach* leaf extract (MLE) for the treatment of tomato wilt, with the optimal conditions determined to be 1100 W MW power, 30 s irradiation time, and water as the solvent.[132] The concentration of $AgNO_3$ and MLE extract was also optimized for the process. In a study Maryani *et al.*, they synthesized Ag NPs using *Desmodium triquetrum* as a reducing and stabilizing agent. The Ag NPs demonstrated significant anticancer activity against MCF-7 breast cancer cells and exhibited potential antibacterial and antibiofilm properties in various *in vitro* assays.[133] In another study, Devasvaran *et al.* used MAS for the preparation of Ag NPs using *Clinacanthus nutans*, a tropical Asian plant, based on crude polysaccharide extract.[134] Here, the size of the fabricated Ag NPs was approximately 5.3 nm. The variation in the size of synthesized Ag NPs could be observed in many studies involving the MAS-based approach using plant extracts. For example, Jahan *et al.* utilized *Rosa santana* (rose) petals,[135] while Tormena *et al.* explored *Handroanthus impetiginosus* extract.[136] In both cases, the average size was in the range of approximately 15–23 nm. The study reported by Ulusu *et al.* utilized *Cistus salviifolius* L. and *Ferula communis* L. for the synthesis of Ag NPs with a size of ~11 nm.[137] Numerous reports have been encountered on the MAS-based synthesis of Ag NPs using a variety of plant extracts.[138–144] However, in all cases, the irradiation time and power differ. A comparison of the size distribution of fabricated Ag NPs using various green approach-based MAS is presented in Fig. 5(a–e).

The size and shape of the fabricated NPs depend on the choice of regulatory parameters while exploring MAS. Uniform heating is a key aspect of MAS, which in turn is affected by many factors, including the selection of MW frequency, power, time, and choice of solvent. In general, it is observed that NPs synthesized in the solution phase are easily regulated compared to reactions *via* solid-phase synthesis. This be attributed to the uniform heat circulation and shielding of solvents from MWs. Although a direct mechanism for MAS synthesis has not been formulated, it has been observed that an increment in the irradiation time leads to the production of NPs with a comparatively small size. This trend is governed by many parameters, and thus it is necessary to study and examine the effect of each parameter separately to present a concrete mechanism.

A green synthetic approach has also been used in designing composite NPs, including noble metals. In a study by Vijayan *et al.*, they fabricated both Ag and Au NPs using *Myxopyrum serratulum* leaf extract, which acted as both a reducing agent and stabilizer. The MW approach significantly reduced the synthesis time by enabling uniform heating, accelerating the completion of the reaction.[145] MAS has also been used as an innovative approach to fabricate NP-based fillers in hydrogels. In a study reported by Aldakheel *et al.*, a chitosan-PVA hydrogel incorporating Ag NPs was synthesized using MW irradiation to accelerate the reduction of Ag ions by the chitosan-PVA mixture, enabling the rapid formation of a hydrogel with encapsulated Ag NPs.[146] This not only allowed the rapid synthesis of hydrogel scaffolds but also increased their physicochemical and mechanical features. Further, biocompatible Au NPs with anticancer property against human glioma (LN-229) cells were synthesised by Adnan *et al.* while exploring the use of kenaf seeds.[147] In this study, it was demonstrated that the use of kenaf seeds acted as both reducing as well as supporting agents for Au NPs fabrication. The ability of plant extract to act as both a reducing as well as stabilizing agent for fabricating noble metal NPs was further examined by Shakibaie *et al.*, who synthesized Pt NPs using an aqueous extract of *Eucalyptus camaldulensis.*[148] The fabricated Pt NPs demonstrated significant antioxidant activity and exhibited excellent cytocompatibility *in vitro* against breast cancer (MCF-7) and lung cancer (A549) cell lines. Similarly, Priyadharshini *et al.* synthesised macroalgae *Gracilaria edulis* extract-stabilised Ag NPs and ZnO NPs using MW irradiation.[149] The synthesised NPs were found to possess a comparable size of ~100 nm. In this study, a cytotoxicity analysis was performed on PC3 cells, which revealed that the ZnO NPs exhibited better anticancer effects than Ag NPs. In a recent study, Kaplan *et al.* synthesized Ag NPs using MW irradiation with crude extracts of *Boletus edulis* and

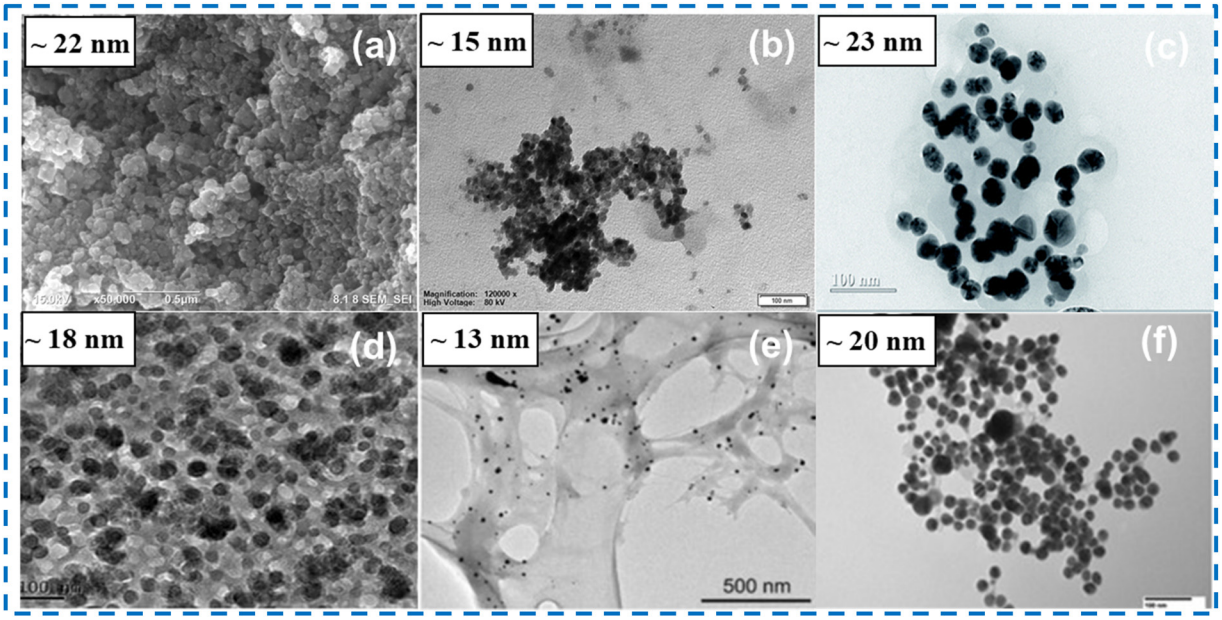

Fig. 5 (a–f) Comparison of the size of different Ag NPs fabricated using MW-assisted synthesis. (a) Reproduced from ref. 133 with permission from The Royal Society of Chemistry, Copyright 2022, (b) reproduced from ref. 135 with permission from Taylor & Francis, Copyright 2019, (c) reproduced from ref. 136 with permission from The Royal Society of Chemistry, Copyright 2020, (d) reproduced from ref. 138 with permission from MDPI, Copyright 2023, (e) reproduced from ref. 141 with permission from Elsevier, Copyright 2023, and (f) reproduced with permission from ref. 144 with permission from MDPI, Copyright 2024.

Coriolus versicolor.[150] The cytotoxicity analysis confirmed their strong anticancer potential, while additional assays demonstrated their excellent antimicrobial and wound-healing properties (Fig. 6(a)). Moreover, Seku *et al.* reported the fabrication of Pd NPs using *Limonia acidissima* Groff gum. The gum facilitated the synthesis of smaller Pd NPs with a size of 0–16 nm, given that the modified gum served as a reducing agent.[151] These Pd NPs were used as a sensing probe to detect glucose, given that the fabricated NPs could mimic peroxidase-like activity. In this case, the fabricated Pd NPs could oxidize tetramethylbenzidine (TMB) substrate and produce gluconic acid and hydrogen peroxide (H_2O_2) when glucose oxidase oxidizes glucose, which could be detected at 652 nm (Fig. 6(b and c)). The choice of NMs and the selection of parameters for their fabrication have to be carefully optimized, given that a trivial change in the synthesis parameters could present broad changes in the size and shape of the fabricated NMs. Given that the shape and size directly influence the efficiency of NMs in many biomedical applications, optimization of the MAS approach is a crucial step. Further, the yield of NMs fabricated using MAS can also be regulated by manipulating its parameters.

MAS-based approaches have been explored for different types of NPs, where regulating the parameters of MW irradiation plays a crucial role. In a study, copper NPs (Cu NPs) were synthesised by Jahan *et al.* using *Citrus sinensis* juice extract, which is rich in ascorbic acid (vitamin C).[152] These NPs exhibited potent antibacterial activity against *S. aureus*, while being highly cytocompatible, as evaluated against fibroblast cells. Bactericidal Cu NPs with a size of 15 nm and a high degree of stability up to four months were fabricated by another research group.[153] Identically, copper ferrite NPs ($CuFe_2O_4$ NPs) were fabricated with TiO_2 and reduced graphene oxide coating, and subsequently examined for application in magnetic hyperthermia.[154] In a separate study, Shakibaie *et al.* synthesised cadmium NPs (Cd NPs) using MWs, visualised as hexagonal structures of approximately 20 nm, which possessed ROS scavenging activity comparable to vitamin C.[155] The as-fabricated Cd NPs exhibited excellent compatibility, whereas Zn NPs synthesised in the same study along similar lines demonstrated a protective effect against cisplatin-induced toxicity.[156] Asplatin (prodrug of aspirin and cisplatin) encapsulating Zn NPs were synthesised using gambogic acid, which were found to be cytotoxic against chemoresistant breast cancer cells.[157,158] A similar approach was used elsewhere for the synthesis of ZnO NPs using *Pistia stratiotes*[159] and *Lactobacillus plantarum.*[160] MAS enables the development of reproducible, stable NPs without the need for the addition of harmful chemicals during the synthesis. Additionally, Ameri *et al.* fabricated palladium NPs (Pd NPs) under MW utilising vitamin C and sodium alginate, obtaining NPs with a size in the range of 13–30 nm with excellent reduction capabilities.[161] Further, a recent study by Alkhalidi *et al.* reported the fabrication of Pd NPs using acid protease extracted from *Melilotus indicus* leaf extract using MW irradiation for 45 min at 800 W.[162] It was observed that a prolonged irradiation time led to smaller Pd NPs, with little impact on the maximum size. Moreover, in the case of selenium nanocrystals (Se NPs) syn-

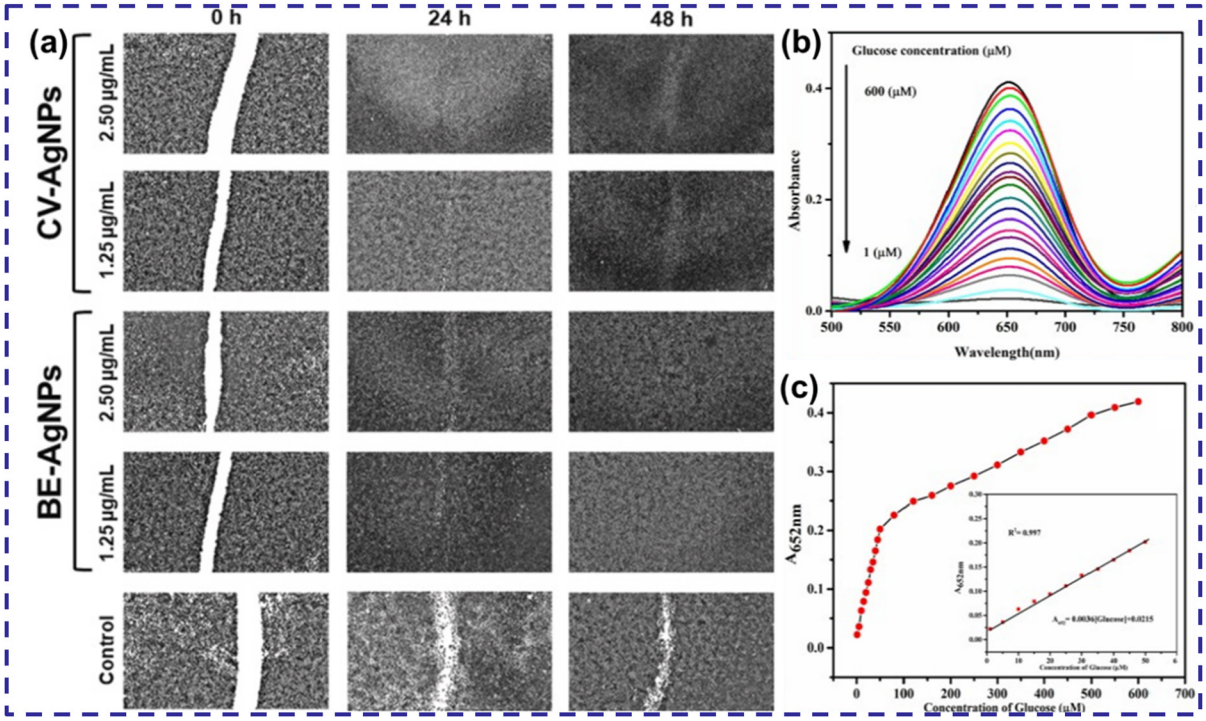

Fig. 6 (a) *In vitro* wound healing activity of 2.50 μg mL^{-1} and 1.25 μg mL^{-1} of Ag NPs fabricated using MW irradiation with crude extracts of *Coriolus versicolor* (CV-AgNPs) and *Boletus edulis* (BE-AgNPs) in the L929 cell line for 24 h and 48 h,[150] (b) UV-vis absorption spectra of various concentrations of glucose and (c) plot showing glucose concentration as a function of absorbance maximum at 652 nm; inset demonstrates the linear curve.[151] (a) Reproduced from ref. 150 with permission from Elsevier, Copyright 2021 and (b and c) reproduced from ref. 151 with permission from Elsevier, Copyright 2024.

thesised *via* reduction and stabilisation using various plant extracts, size-dependent aggregation was noted.[163] Moreover, Se NPs fabricated using MAS were also stabilized by chitosan in a separate study by Zidan *et al.*, where a rapid color change was observed, confirming the formation of Se NPs.[164] Further, Mellinas *et al.* developed ROS scavenging Se NPs using *Theobroma cacao* extract *via* MAS, which exhibited high stability till 55 days at 4 °C.[165] In a separate study, *Ephedra pachyclada* Boiss. extract-stabilised arsenic NPs (As NPs) were fabricated using MAS, highlighting the significance of the precursor in the NP formation.[166]

MAS was exploited as a method for the design and synthesis of novel tumor-derived microparticles by Wu *et al.*, thereby bypassing the low efficacy and safety encountered using the conventional UV irradiation method.[167] These extracellular vesicles triggered immunogenic response-driven cell death, while simultaneously modulating the tumor microenvironment, thereby acting as a dual-edged sword against lung adenocarcinoma. MAS has also been explored in the manufacturing of lipid NPs, such as non-ionic surfactant vesicles and bilosomes by Gebril *et al.* for the incorporation of tetanus toxoid inside the lipid NPs.[168] It was revealed that bilosomes could entrap more of the toxoid, and the orally administered bilosomes exhibited the best immunisation, as validated by the augmented IgG levels. Additionally, Dunn *et al.* fabricated lipid NPs using fatty acid triglycerides and vitamin E *via* MAS.[169] The NPs demonstrated excellent long-term stability, which could be due to the van der Waals forces and stearic repulsion between the particles. MAS massively reduced the synthesis time to almost a minute, with 20–30 nm transparent particles being formed. It should be noted that although the choice of precursor is crucial in deciding the fate of the fabricated NPs, along with MW-dependent parameters, sometimes the interatomic behaviour of the fabricated NPs is not affected much by the change in the surrounding environment.

3.3. Microwave-assisted synthesis of nanostructures combined with other fabrication techniques

Metal and metal oxide NPs can be synthesized using hydrothermal or solvothermal methods combined with MW irradiation, which accelerates the reaction and reduces the synthesis time. To explore this, Garino *et al.* demonstrated the synthesis of ZnO/functionalized ZnO nanocrystals using both the conventional solvothermal and MW-assisted techniques.[170] In both methods, a zinc precursor was converted to ZnO NPs *via* reduction with a hydroxide salt. The MW-assisted process employed a Teflon reactor with temperature and pressure probes, whereas the conventional method used a reflux setup with constant heating and stirring. The MW technique produced stable nanocrystals with a uniform size and shape (Fig. 7(a and b)), which exhibited cytotoxicity and consistent cellular uptake in KB cancer cells. In a separate study by Arani

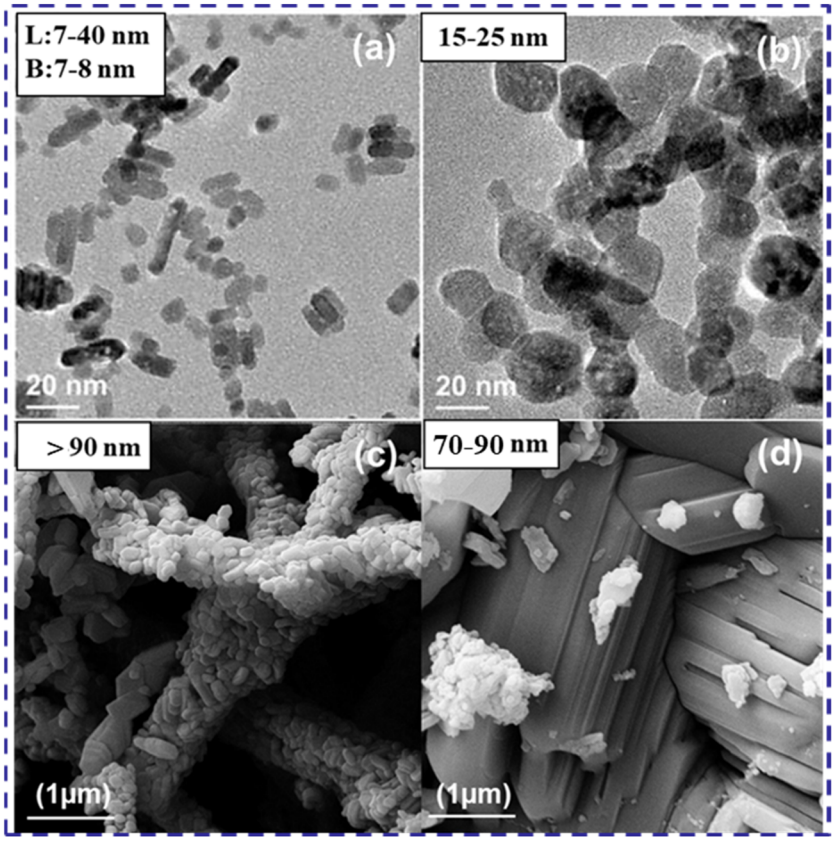

Fig. 7 High-resolution transmission electron microscopy images of (a) ZnO nanocrystals, synthesized through conventional wet chemical method, (b) amino-functionalized ZnO nanocrystals, synthesized through a MW-assisted route[170] and MoO_3 fabricated by (c) MW-assisted synthesis and (d) conventional wet chemical method.[171] (a and b) Reproduced from ref. 170 with permission from MDPI, Copyright 2019 and (c and d) reproduced from ref. 171 with permission from Elsevier, Copyright 2020.

et al., the wet chemical method and MAS approach were compared for the fabrication of molybdenum trioxide NPs (MoO_3 NPs).[171] It was demonstrated that MAS of MoO_3 nanostructures resulted in arranged nanorods decorated with NPs, whereas wet chemical synthesis resulted in aggregates of NPs (Fig. 7(c and d)). The use of MAS for the preparation of NMs/NPs presents a high rate of energy to the reaction mixture compared to the conventional heating approach. This could result in altered reaction kinetics and atomic movements in the solution, resulting in different morphologies compared to conventional routes.

In contrast, Srinivasan *et al.* fabricated cobalt-encapsulated CaP NPs using MAS followed by thermal annealing.[172] In the first step, MW irradiation was done at 900 W for 30 min followed by the next step, which includes thermal annealing in the range of 200–1000 °C. It was demonstrated that the heating altered the NP morphology from spherical to twinned shapes. The effect of annealing after MAS of bredigite NPs was also demonstrated by Kheradmandfard *et al.*, where post-MAS of NPs, heat treatment was performed for 2 h in the range of 900–1300 °C.[173] In this study, the uniform distribution of NPs was observed at the highest annealing temperature. Similarly, in a separate study, forsterite nanopowder of ~100 nm was fabricated using MAS using 850 W MW with 15 min of irradiation, followed by heat treatment @ 10 °C min^{-1} up to 800 °C for 2 h.[174] The MAS of NMs and NPs could also be linked with different fabrication techniques, such as the hydrothermal approach. To validate this, Qi *et al.* fabricated nanospheres of amorphous calcium carbonate (ACC) and amorphous calcium phosphate (ACP) using a hydrothermal MW approach.[175] Here, the reaction mixture for ACC/ACP nanospheres was placed in a hydrothermal setup and placed in a MW for 10 min at 110 °C. The hydrothermal conditions provide a constant pressure to the reaction mixture, whereas MAS provides uniform heating, which could aid in enhancing the stability of the fabricated nanospheres. Considering these points, Zhao *et al.* assembled flower-like hierarchical nanostructures of individual hydroxyapatite (HAp) nanosheets.[176] The reported study also explored the hydrothermal MW approach (100 °C for 5 min). Here, an increase in the temperature up to 200 °C resulted in minimal flower-like nanosheet assembly, while the majority of the product was comprised of individual nanosheets. Temperature has a vital effect on the crystal phase and morphological assembly of individual NPs. Changing the temperature results in a variation in the movement of atoms in the solution and affects the reaction kinetics. These changes affect the morpho-

logical assembly of NPs, giving them certain shapes. The effect of MW power and irradiation time on the size of different NPs for a particular solvent has been summarized in Table 1.

3.4. Effect of solvent on the synthesis of nanostructures using the microwave approach

Solvents play a crucial role in chemical and manufacturing processes. Their selection significantly impacts economic, environmental, and societal outcomes. Similarly, solvents play a vital role in MW-assisted liquid-phase synthesis, particularly in the synthesis of NSs. Solvent polarity is critical in MW-assisted synthesis, given that higher polarity enhances MW energy absorption, increasing the temperature and reaction rate.[65] MW-assisted chemical processes utilize dielectric heating, where polar molecules absorb and convert MW radiation into heat. MW radiation induces electrical dipoles in polar molecules, causing them to reorient with the oscillating electric field continuously. Heat is generated due to dielectric polarization, conduction loss, and molecular friction as molecules reverse direction. The loss factor ($\tan\delta$) quantifies the efficiency of a solvent in converting MW energy into heat.[186] The loss tangent ($\tan\delta$) quantifies the ability of a material to absorb MW radiation at a specific frequency and convert it into heat. It is calculated as the ratio of the imaginary part (ε'') to the real part (ε') of the complex dielectric permittivity (ε^*). Tan δ varies with temperature and irradiation frequency. The loss factor (ε'') represents the efficiency of converting electromagnetic energy into heat, while ε' measures the capacity of a material to store electrical potential energy in an electric field.[187] Solvents are categorized as strong, medium, or weak MW absorbers based on their loss factor ($\tan\delta$). Higher $\tan\delta$ values enable faster and more efficient MW heating, while low $\tan\delta$ values result in slower and less effective heating under MW irradiation.[188]

Nonpolar solvents such as carbon tetrachloride and dioxane are MW-transparent due to the absence of a permanent dipole moment. In MAS, strongly polar substrates, reagents, or catalysts must be introduced to enhance the dielectric properties of the reaction medium.[189] Alcohols are widely used in the MAS of various inorganic NSs due to their high loss tangent ($\tan\delta$) values. In addition, ethanol has a $\tan\delta$ of 0.941 at 20 °C and 2.45 GHz, which is significantly higher than that of water of 0.123 at ambient temperature, making alcohols exceptional MW absorbers. The commonly used alcohols possess relaxation properties that enable effective coupling with MW frequencies, making them ideal solvents for MW heating. MW heating in organic solvents such as ethanol relies on dipolar polarization, but an increase in temperature reduces the MW absorption due to the lower viscosity as well as molecular friction. Polyalcohols, for example, ethylene glycol ($\tan\delta$ = 1.350 at 2.45 GHz, 20 °C), glycerol, 1,3-propanediol, and 1,4-butanediol, are ideal for MAS of NSs due to their high loss tangents. Their ability to form extensive hydrogen bonds results in high viscosity and long relaxation times. Ethylene glycol, with its higher dielectric loss as well as boiling point comparable to water, is extensively used in MAS. It achieves faster heating rates and higher temperatures in open systems compared to some hydrothermal methods.[190] Soltani *et al.* demonstrated that ZnS nanocrystals synthesized *via* the MW–polyol method exhibited greater crystallinity compared to the MW-hydrothermal method in water.[191] The polyol process employs polyols as both the solvent and reductant, eliminating the need for additional reducing agents, unlike the synthesis of metal NSs in aqueous solutions.[192] Beyond water and polyols, various solvents have been explored for the MW-assisted synthesis of NSs, broadening the scope of MW heating in the production of nanomaterials. Especially, in MAS of inorganic NSs, diverse organic solvents have been utilized, including alcohols, low-molecular-weight PEG, ethylene glycol monoalkyl ethers, DMF, hexane, nonadecane, methacrylate, trioctylphosphine, DMSO, acetonitrile, THF, formaldehyde, and cyclohexanone.[190] Ionic liquids are increasingly used as green media for inorganic synthesis due to their unique properties, including high thermal stability, negligible vapor pressure, broad liquid-state temperature range, low interfacial tension, and high ionic conductivity.[193] The structure and ionic compositions of these ionic liquids influence their characteristics. Additionally, ionic liquids are especially excellent MW absorbers due to their high polarizability and responsiveness to irradiation. MW heating with ionic liquids enables the faster and more energy-efficient synthesis of nanostructured materials compared to conventional methods. Ionic liquids facilitate MW-assisted reactions even in nonpolar solvents. In this regard, Leadbeater *et al.* demonstrated that adding a small amount of 1,3-dialkylimidazolium iodide to hexane significantly enhanced the reaction rates and yields, achieving a temperature of 217 °C after 10 s of MW heating at 200 W.[194] Ionic liquids, such as 1-butyl-3-methylimidazolium hexafluorophosphate ([bmim][PF_6]), are efficient MW absorbers due to ionic conduction. Their $\tan\delta$ increases with temperature, from 0.185 at 20 °C to 1.804 at 100 °C, and further to 3.592 at 200 °C, making them effective across a wide temperature range. Furthermore, in the MW-assisted ionic liquid synthesis of metal oxide NSs, a metal compound acts as the metal source, an alkaline reagent creates an alkaline environment, and additives or surfactants are sometimes used to control the morphology and size.[195] Each solvent has characteristic features, which are crucial in its selection for the MAS of NSs, as summarized in Table 2.

3.5. Role of mixed solvents in microwave-assisted synthesis of nanostructures

The characteristics of solvents significantly influence and regulate the morphological and structural attributes of the synthesized NSs during MW heating. Each solvent has its own approach for interaction with MWs owing to variations in polarity, dielectric properties, and internal architecture. MAS with mixed solvents offers enhanced control over nanostructure formation compared to single-solvent methods. By selecting multiple solvents and adjusting their volume ratios, mixed systems can regulate the size, chemical composition, structure, and morphology of the end product. MW heating,

Table 1 Effect of microwave power and irradiation time on the size of fabricated NPs

S. no.	Nanoparticle system	Size (nm)/ instrument	MW power, irradiation time	Reagents used	Solvent	Application/cell line and/or bacterial and antifungal stain	Ref.	Remarks on trends
1	Ag NPs	~22/SEM	900 W; 1.5 min	- Ag NO_3 (2 mM) - *Desmodium triquetrum* DC extract	Water	Antibacterial and anticancer/ MCF-7cells/*B. subtilis*, *P. aeruginosa*, *E. coli* and *K. pneumoniae*	133	High power and short time → small monodisperse NPs
2	Ag NPs	~14/TEM	300 W; 25 min	- $AgNO_3$ (1 mM)	Water	Antibacterial/L929 cells/*S. aureus* and *E. coli*	135	
3	Ag NPs	~13.4/TEM	800 W; 15 min	- Rose petal extract - *Handroanthus impetiginosus* (Mart. ex DC.)	Water	Antimicrobial/Human keratinocyte (HaCat) cells/*S. aureus* and *E. coli*	136	
4	Ag NPs	~10/TEM	NA; NA	- Mattos underbark extract - 1.0×10^{-3} mol L^{-1} $AgNO_3$ solution - *Cistus salviifolius* L. extract - *Ferula communis* L. extract - 10 mM $AgNO_3$ solution	Water	Antioxidant, antibacterial, and cytotoxic/lung cancer A459 cells	137	
5	Ag NPs	~18/TEM	350 W; 10 min	- 0.001 M Ag NO_3 - *H. arnottiana* leaf extract	Water	Antimicrobial, and anticancer/Dalton's lymphoma ascites (DLA) cells/*E. coli*, *K. pneumoniae*, *S. aureus*	138	Medium power, time → improved size and efficacy
6	Ag NPs, Cu NPs, Ni NPs	~136/DLS	450 W; NA	- *A. tuncelianum* extract-10 mM AgO_3 - 10 mM $CuSO_4$ - 10 nM NiSO	Water	Anti-amoebic activity/ *Acanthamoeba castellanii*	139	
7	Ag NPs	10–20/TEM	800 W; 10 min	- *Capparis moonii* extract - 1 mM $AgNO_3$	Water	Anticancer/L929, MCF-7, A549, pancreatic (PANC-1) cells and human skin (A431) cells	140	
8	Ag NPs	~13/TEM	500 W; 180 min	- Cellulose nanocrystal - $AgNO_3$ (0.1 M)	Water	Antibiofouling/*S. aureus*, *S. saprophyticus*, *E. coli*, *P. aeruginosa*, and *S. epidermis*	141	
9	Ag NPs	~100/TEM	800 W; 1 min	- Algae bloom extract - 1 mM $AgNO_3$	Water	General/melanoma (A375) cells, A549, colorectal carcinoma (Caco-2) cells, and vero normal cells	142	
10	Ag NPs	~13/TEM	NA; 6 h at 5 bar at 100 °C or 10 min at 5 bar and 100–120° C	- Lignin - $AgNO_3$ solution	Water, 1 M HCl	Antibacterial/ monocytic THP-1 cells/MDR *P. aeruginosa*, and methicillin-resistant *S. aureus*	143	

Table 1 *(Contd.)*

S. no.	Nanoparticle system	Size (nm)/ instrument	MW power, irradiation time	Reagents used	Solvent	Application/cell line and/or bacterial and antifungal stain	Ref.	Remarks on trends
11	Ag NPs	~20/TEM	NA; 2, 5, 10 and 20 min	- *Houttuynia cordata* extract - 10 mM $AgNO_3$ solution	Water	Antibacterial, and antifungal/*E. coli*, *P. aeruginosa*, *A. baumannii*, *S. aureus*/*C. albicans* and *T. rubrum*	144	
12	Ag NPs, and Au NPs	~37 and ~16/TEM	800 W; 1 min	- 1 mM $AgNO_3$ solution or - 1 mM $HAuCl_4{\cdot}3H_2O$ solution - *Myxopyrum serratulum* leaf extract	Water	Antibacterial, antioxidant, and catalyst	145	
13	Ag NP-incorporated chitosan and PVA-based hydrogels	~22/DLS	800 W; 10 min	- Chitosan - PVA - KPS (initiator) - MBS (cross-linker) - Silver nitrate	Water	Wound healing/ mouse skin fibroblast (L929) cells	146	
14	Au NPs	5–20/TEM	800 W; 90 s	- *Hibiscus cannabinus* extract - $HAuCl_4$ (1 mM) solution	Water	Anticancer/mouse macrophage (RAW 264.7) cells, mouse fibroblast (NIH3T3) cells and human glioma (LN-229) cells	147	Swift synthesis → uniform small NPs
15	Ag NPs and Zn NPs	55–99 and 6–95/TEM	NA; 10 min	- *Gracilaria edulis* extract - $AgNO_3$ solution (1 mM) - Zinc nitrate (1 mM)	Water	Anticancer/human prostate cancer (PC3) cells	149	Longer synthesis time → higher particle size and cytotoxicity
16	Ag NPs	~ 86/DLS	475 W; 2 min	- *Boletus edulis* and *Coriolus versicolor* extracts - NaOH - $AgNO_3$ solution (10 mM)	Water	Antimicrobial, anticancer, and wound healing/L929, MCF-7, HT-29 and HUH-7 cell/*P. aeruginosa*, *K. pneumonia*, *S. aureus* and *E. faecalis*	150	
17	Au NPs	7–9/TEM	650 W; 150 s	- Carboxymethylated *Frankincense* resin - 1 mM $HAuCl_4$ solution	Water	Antibacterial, antioxidant and anticancer/HeLa cells/ *S. aureus*, *E. coli* and *K. pneumoniae*	177	
18	Cu NPs	7–21/TEM	700 W; 5 min	- 1 mM copper(II) sulfate pentahydrate solution	Water	Antibacterial/*E. coli* and *S. aureus*	152	Medium synthesis time → stable efficacious NPs
19	$CuFe_2O_4$@TiO_2@rGO	~60/SEM	850 W; 12 min	- Orange juice extract - *Pedalium murex* leaf extract - Copper nitrate	Ethanol	Anticancer/ MDA-MB-231cells	154	

Table 1 *(Contd.)*

S. no.	Nanoparticle system	Size (nm)/ instrument	MW power, irradiation time	Reagents used	Solvent	Application/cell line and/or bacterial and antifungal stain	Ref.	Remarks on trends
20	Cadmium NPs (Cd NPs)	~15/SEM	850 W; 15 s	- Ferric nitrate (1 : 2 molar ratio) - *Artemisia persica* extract	Water	General/A549, 3T3, HT-29, MCF-7, and U87 cells	155	
21	Zn NPs	~50/SEM	850 W; 60 s	- 7.7 mM Cd $(NO_3)_2{\cdot}4H_2O$ - *Lavandula vera* leaf extract - $ZnSO_4$ (1 mM) solution	Water	Testicular toxicity/*In vivo*	156	
22	Zn NPs	20–100/ TEM	340 W; 8 min	- $Zn(NO_3)_2{\cdot}6H_2O$ - *Citrullus colocynthis* (L.) Schrad extract	Water	General/3T3 cells/*B. subtilis*, methicillin-resistant *S. aurous*, *P. aeruginosa*, and *E. coli*	157	
23	Zinc (Zn NPs)	55–85/TEM	NA; 5 min (30 s per cycle)	- Zinc acetate dihydrate - Gambogic acid	Water	General/human breast cancer (MDA-MB-231) cells	178	
24	ZnO NPs	~ 537/DLS	1000 W; 3 min	- *Lactobacillus plantarum* broth	Ethanol, water and NaOH solution	Antibacterial/ methicillin-resistant *S. aureus*	160	Higher power → Increase in crystalline size and improved efficacy
25	Pd NPs	18–30/TEM	850 W; 3 min	- $[Zn(CH_3COO)_2]{\cdot}2H_2O$ - Ascorbic acid - Sodium alginate	Water	Antioxidant/ fibroblast-like (HSkMC) cells and A549 cells	161	Reduced irradiation time → stable NPs with smaller size
26	Pd NPs	~5–30/ TEM	800 W; 45 min	- 1 mM palladium(II) acetate solution - *M. indicus* leaf acid protease - 0.01 M $C_4H_6O_4Pd$ solution	Water	General/MCF-7 cells/ *E. coli*	162	
27	Se NPs	12–22/TEM	600 W; NA	- Na_2SeO_3 solution (30 mM) - *Coccinia grandis* fruit extract	Water	Antibacterial/*E. coli*, *B. cereus*, and *S. aureus*	163	
28	Selenium (Se NPs)	~11/TEM	900 W; 15 min	- Na_2SeO_3 - Chitosan - SDS	Water, acetic acid	Anticancer, Antibacterial/human breast cancer (MCF-7) cells & *P. aeruginosa*, *E. coli*, *S. aureus*, and *B. subtilis*	164	
29	Se NPs	10–20/TEM	900 W; NA	- Citric acid - Sodium alginate	Water	Antioxidant, Antimicrobial, and Anticoagulant/MCF-7 cells/*E. coli*, *P. aeruginosa*, *B. subtilis*, and *S. aureus*	179	

Table 1 *(Contd.)*

S. no.	Nanoparticle system	Size (nm)/ instrument	MW power, irradiation time	Reagents used	Solvent	Application/cell line and/or bacterial and antifungal stain	Ref.	Remarks on trends
30	Arsenic (As NPs)	~51/TEM	850 W; 60 s	- Na_2HAsO_4 solution (1 mM) *E. pachyclada* Boiss extract	Water	Antioxidant, and Anticancer/A549, MCF-7, HT-29, glioblastoma (U87) cells, and Mouse embryonic fibroblast (3T3) cells	166	Fast synthesis → moderate particle size and high efficacy
31	Ag NPs	~17/TEM	800 W; 5, 10 and 15 min	- *Pelargonium sidoides* - DC extract - 1.0×10^{-3} mol L^{-1} - $AgNO_3$ solution	Water	Antibacterial/*S. aureus* and *E. coli*	180	
32	Ag NPs	~5/SEM	NA; 5 min	- $AgNO_3$ (10 mM) - *Clinacanthus nutans* leaf extract	Water	General/MCF-7 cells	181	
33	Ag NPs	~134/DLS	NA	- $AgNO_3$ solution - Saponin mixture	Water	Anticancer/A549 cells	182	
34	Ag NPs	~65/SEM	1200 W; 2 min	- *Pimpinella anisum* L. fruit extract - 5 mm $AgNO_3$ solution	Water	Antibacterial, and Cytotoxic/MCF-7, colon carcinoma (HT-29) cells, human keratinocytes (HaCaT) cells, and Embryonic kidney (HEK-293) cells/*B. subtilis*, *S. aureus*, *E. faecalis*, and *E. coli*	183	
35	Zinc oxide (ZnO NPs)	~35/SEM	400 W; 30 min	- Zinc nitrate hexahydrate (0.1 M) - *Euterpe oleracea Mart.*	Water	Antioxidant, antibacterial, and anticancer/ keratinocyte (HaCaT) cells/*S. aureus*, *E. coli*, *P. aeruginosa*, and *K. pneumoniae*	184	
36	Copper oxide (CuO NPs)	~ 135/TEM	NA; 5 min (30 s per cycle*10 cycles)	- Copper acetate monohydrate - *Boswellia carterii* essential oil	Water	Anticancer/colorectal cancer (HCT-116) cells	185	
37	Pt NPs	~7–11/SEM	850 W; 1 min	- 1 mM $H_2PtCl_6{\cdot}6H_2O$ solution - *Eucalyptus camaldulensis* extract	Water	Cytotoxicity analysis in MCF-7, A549 cells	148	
38	Ag NPs	12–46/SEM	1100 W; 30 s	- $AgNO_3$ solution (2.5 mM) - *Melia azedarach* leaf extract	Water	General/*Fusarium oxysporum*	132	

especially in binary solvent systems with polar as well as non-polar solvents, enables phase-specific temperature control. In an MW-assisted phase transfer process, water can reach up to 100 °C, although chloroform remains beneath its boiling point (~61 °C), facilitating reactant extraction between phases.[190] Polyols, containing multiple –OH groups, are highly effective for MW heating due to their high loss tangent (tan δ) values and superior MW absorption compared to water. Mixing polyols with water enhances the MW absorption, while improving the solubility of reactants, especially those with high molecular weights. Polyols are extremely miscible with water and always tend to form intermolecular hydrogen bonds, resulting in high viscosity. Adding water to polyols reduces their viscosity and increases the reactant solubility.[198] MAS of metal NSs using ethylene glycol (EG) and water as solvents has been highly effective. Alcohol serves as an effective solvent specifically for MW heating, given that it absorbs MWs more efficiently compared to water. The combination of alcohols and water

Table 2 Characteristic features of different solvents in the MAS of nanostructures

Solvent	Tan δ at 20 °C (2.45 GHz)	Boiling point (°C)	Key characteristics	Ref.
Water	0.123	100	• Polar, low viscosity • Limited MW absorption at high temperatures	190
Ethylene glycol (EG)	1.350	197.3	• High loss tangent, forms • Hydrogen bonds • Widely used in MW-assisted synthesis	190
1,3-Propanediol	~ 1.350	214	• High viscosity • Effective for MW • Heating	196
Benzyl alcohol	0.330	205	• Moderate polar solvent • Often used in mixed solvent systems	189
Ethanol	0.941	78.3	• Polar • Effective MW absorber at low temperatures • Reduced absorption at higher temperatures	190
Glycerol	0.650	290	• High viscosity • Strong hydrogen bonding • Used in polyol synthesis	196
DMSO	0.825	189	• Strong polar solvent • Excellent MW absorber	187
DMF	0.165	153	• Moderate MW absorber • Miscible with water • Limited reports in mixed solvent use	187
Hexane	~0.020	69	• Nonpolar, MW transparent • Low reactivity	194
1-Butyl-3-methylimidazolium hexafluorophosphate ([bmim][PF_6])	0.185 at 20 °C, 3.592 at 200 °C	Ionic liquid	• Exceptional MW absorber due to ionic conduction • Tunable polarity	195
Toluene	~0.040	110.6	• Nonpolar • MW transparent • Results in larger particle sizes in nanostructure synthesis	197

enhances MW absorption compared to water alone. Alcohols readily mix with water and can form intermolecular and intramolecular hydrogen bonds. Due to their low boiling points, alcohols, especially those with lower molecular weights, are suitable for low-temperature reactions in open systems. In the case of higher-temperature MW-assisted synthesis, solvothermal reactions are necessary in closed systems.[190] There are a few reports on MW-assisted nanostructure formation using mixed solvents, including *N*,*N*-dimethylformamide (DMF)[199] and water or water mixed with 1,2-ethylenediamine.[200] The mixed solvents with diverse polarities act as a heat sink that draws the thermal heat away from the reactants. However, adequate care has to be taken while selecting the binary system as a significant polarity difference could sometimes lead to the development of by-products that could interfere with the purity of the NMs to be fabricated.

3.6. Influence of solvent-substance interactions on microwave-assisted synthesis of nanostructures

Solvent-substance interactions govern nanostructure processes, including dissolution, formation, growth, assembly, and structuring. Controlling these interactions is essential for tailoring NSs with specific morphologies for applications in catalysis, sensing, biomedical technology, and their further use in the conversion of energy. The polarity of the solvent significantly influences various properties, such as shape and size, of the synthesised NSs by affecting their nucleation, growth, and surface chemistry. Solvents with high polarity, for example, water and alcohols, stabilize the surface of NSs, promoting well-defined morphologies and sizes. In aqueous solution, water molecules form a stabilizing layer around NSs, preventing their agglomeration.[201–203] Experimental results indicate that the solvent polarity significantly influences the size and shape of tellurium NSs. Solvents with high polarity promoted the synthesis of NPs that were small in size, while solvents with lower polarity, such as ionic liquids, encouraged the synthesis of larger structures.[204] Ionic liquid with variable polarity enable precise control over the morphology and size of tellurium structures. Solvent polarity, particularly in water, alcohol, and ionic liquids, significantly influences the formation of tellurium nano- and micro-structures. Ionic liquids offer the advantage of customizable polarity, allowing tailored control over the formation of tellurium structures. Nonpolar solvents, such as toluene and hexane, promote the formation of larger NSs due to their lower surface energy. Nonpolar solvents such as toluene and hexane, characterized by their lower surface energy, facilitate the synthesis of bigger NSs. These specific solvents reduce the stability of the surface, causing NMs to agglomerate into larger clusters.[197] Additionally, solvents that are nonpolar in nature are less effective at precursor dis-

solution, which leads to slower reactions and synthesis of NSs that are larger in size.[205] The choice of solvent influenced the aggregation and organization of NSs, leading to distinct assembly structures. Polar solvents produced precise superstructures, including chains and clusters, while solvents that are nonpolar resulted in disordered and specifically random assemblies.[206] The polarity of solvents directly affects the morphology and size of the synthesized NSs, which is summarized in Table 3.

4. Application of microwave-assisted synthesis of nanostructures

MAS of nanostructures has gained significant attention due to its efficiency, versatility, and broad range of applications. This technique stands out owing to its ability to drastically reduce the processing times and energy consumption, while enhancing the reaction kinetics. By enabling rapid, uniform heating, MW-assisted methods offer superior control over the size, shape, and composition of NMs, which is crucial for tailoring their properties for specific applications.[207,208] Unlike conventional methods, which may require multiple steps, MW-assisted synthesis often allows one-step production, making it more cost-effective and scalable.[209–211] As a result, this approach has become a powerful tool for rapidly synthesizing NMs for applications in catalysis, drug delivery, sensors, and energy storage. In addition to these areas, recent advancements have expanded the use of MW-fabricated nanostructures in the biomedical field, including tissue engineering, cancer therapy, and biosensing, where their precise control and enhanced performance can significantly improve therapeutic outcomes.

4.1. Microwave-assisted nanostructures in tissue engineering, regenerative medicine, and infection control

Tissue engineering has emerged as a noteworthy field aimed at developing functional substitutes for damaged or diseased tissues. The integration of NMs, particularly those fabricated *via* MW-assisted techniques, has significantly advanced the development of scaffolds for tissue regeneration. MW-assisted methods offer several advantages for tissue engineering, including rapid synthesis, precise control over material properties, and the ability to create highly porous structures with optimized mechanical and biological characteristics,[46,212]

Nanostructures fabricated through MW energy can be used to create scaffolds that mimic the natural extracellular matrix, providing the necessary support for cell growth and differentiation. These scaffolds can be engineered to exhibit specific properties such as controlled degradation rates, enhanced bioactivity, and mechanical strength, which are crucial for supporting tissue regeneration. Furthermore, the ability to incorporate bioactive molecules, such as growth factors, drugs, and peptides, into MW-assisted scaffolds enhances cell adhesion and promotes tissue healing.

The versatility of MW-assisted techniques also extends to the fabrication of composite materials, combining natural polymers with synthetic NMs to improve the biocompatibility and performance of scaffolds. The rapid and energy-efficient nature of MW synthesis allows the scalable production of these nanocomposite scaffolds, making them suitable for clinical applications in regenerative medicine. Recent advancements in tissue engineering have demonstrated the potential of MW-assisted nanostructures in regenerating a variety of tissues, including bone, cartilage, skin, and nerve tissues.[213–215] As research continues, the use of these NMs promises to accelerate the development of more effective, per-

Table 3 Effect of solvent polarity on the synthesis of nanostructures

Type of solvent	Polarity	Effects on the synthesis of nanostructures	Examples	Ref.
Highly polar solvents	High	- Stabilize nanomaterial surfaces by forming a protective layer. - Prevent agglomeration and promote uniform particle sizes. - Facilitate nucleation and controlled growth of smaller NPs.	Methanol, water, glycerol, ethanol	202 and 203
Low polarity solvents	Low	- Promote the growth of larger particles due to reduced surface stability. - Lead to slower reaction rates and agglomeration into larger clusters. - Less efficient dissolution of precursors.	Toluene, hexane	197
Moderately polar solvents	Medium	- Provide a balance between the dissolution of precursors and controlled growth. - Promote medium-sized nanostructures with moderate stability.	DMF, DMSO, benzyl alcohol	190
Ionic liquids	Variable	- Customizable polarity allows precise control of nanomaterial morphology. - High thermal stability and ionic conductivity Enhance reaction efficiency. - Facilitate the growth of either small or large nanostructures depending on polarity.	[bmim][PF_6], 1-butyl-3-methyl-imidazolium iodide	204
Mixed solvents	Variable	- Combine polar and nonpolar solvents to regulate nucleation, growth, and final morphology. - Enable phase-specific temperature control during synthesis.	Water + alcohol, water + DMF	198 and 199

sonalized therapies for tissue repair and regeneration. Most of the state-of-the-art refers to the generation of silver (Ag),[46,216] zinc oxide (ZnO),[217,218] and HAp NPs,[216,219] and their combination with some scaffold for specific tissue regeneration. For example, Yusoff *et al.* reported the synthesis of silver-incorporated nano-hydroxyapatite particles (Ag-HAp) using a MW-triggered wet precipitation approach. The Ag-HAp composite NPs, with their optimized antimicrobial properties and biocompatibility (Fig. 8(a)), can be used in tissue engineering to promote cell growth, prevent infections, and enhance the regeneration of bone and soft tissues.[216] Similar to Ag, another type of noble metal-based NPs, Au NPs, were loaded onto HAp using a MW-assisted technique, followed by collagen (Col) coating for biomedical applications.[220] The Au-Hap-Col nanostructures achieved ~58.22% drug-loading efficiency and pH-responsive release (~53% at pH 4.5) with doxorubicin. Cytotoxicity studies on MG-63 cells confirmed their non-toxic, bioactive nature, promoting cell growth and proliferation. These results highlight Au-HAp-Col as a favorable material for drug delivery and tissue engineering (Fig. 8(b)). In a recent work, MW-synthesized earth metal ions such as Nd^{3+}, Dy^{3+} co-doped HAp displayed lower cell toxicity and enhanced antimicrobial activities for possible application in photoluminescence and magnetic resonance imaging (MRI) applications.[221]

Carbon dots (CDs) are well-known NMs widely used in various biomedical applications, ranging from bioimaging to tissue engineering.[222] There is a report on a MW-assisted green approach for producing fluorescent silkworm silk with enhanced mechanical properties, using CDs synthesized from citric acid and urea.[223] When added to silkworm feed, the CDs were safely absorbed, leading to the production of silk with increased elongation and strength. The fluorescent silk exhibi-

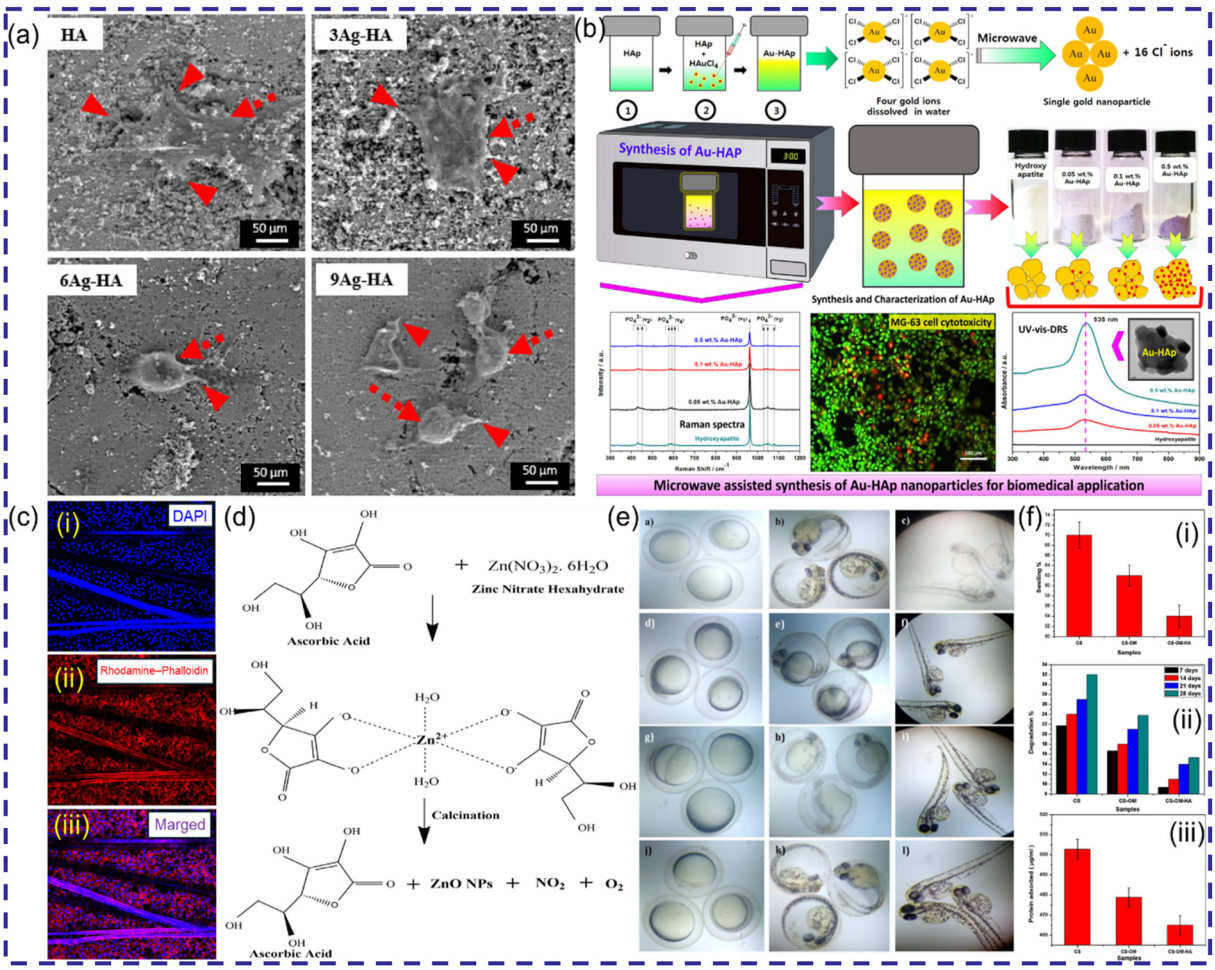

Fig. 8 (a) SEM images showing the *in vitro* biocompatibility of Ag-HAp composite NPs.[216] (b) Synthesis and application of Au-Hap-Col in tissue engineering.[220] (c) (i)–(iii) *In vitro* biocompatibility assay of silk scaffolds synthesized using DAPI and rhodamine-phalloidin staining using L929 cells.[223] (d) Synthesis of ZnO NPs using a MW-assisted method employing ascorbic acid and polyvinyl alcohol as capping and stabilizing agents, respectively.[217] (e) *In vitro* biocompatibility of Co-HAp NRs using a zebra fish model.[224] (f) Characterization of CS-OM-HAp composite scaffolds: (i) swelling behaviour, (ii) degradation profile, and (iii) protein absorption study.[225] (a) Reproduced from ref. 216 with permission from Elsevier, Copyright 2021, (b) reproduced from ref. 220 with permission from Elsevier, Copyright 2019, (c) reproduced from ref. 223 with permission from MDPI, Copyright 2022, (d) reproduced from ref. 217 with permission from Springer, Copyright 2020, (e) reproduced from ref. 224 with permission from Elsevier, Copyright 2021, and (f) reproduced from ref. 225 with permission from MDPI, Copyright 2023.

ted intrinsic blue fluorescence under a 405 nm laser, with no cytotoxicity and excellent cell adhesion (Fig. 8(c)(i–iii)), making it a suitable material for tissue engineering applications. This environmentally sustainable approach also shows potential for the scalable production of high-quality, functional silk for biomedical use. In another study, ZnO NPs were synthesized using a novel MW-assisted method with ascorbic acid and polyvinyl alcohol (PVA) as capping and stabilizing agents (Fig. 8(d)), respectively, resulting in highly crystalline ZnO with a wurtzite structure.[217] The synthesized ZnO NPs, with excellent antimicrobial and photocatalytic properties, show promise for tissue engineering applications by preventing biofilm formation and supporting cell growth and wound healing due to their biocompatibility and antimicrobial activity. In contrast to Ag, Au, and Zn, superparamagnetic mesoporous HAp nanorods (NRs) doped with cobalt (Co) ions have been reported using MAS, with oxalic acid as a chelating agent and black scallop seashells as the calcium source. The resulting Co-HAp NRs exhibit a high surface area, superparamagnetic properties, and excellent antibacterial activity, making them suitable for tissue engineering applications such as targeted drug delivery and cancer treatment. Zebrafish model analysis (Fig. 8(e)) confirmed their low toxicity and biocompatibility, with no significant deformities or malformations, demonstrating their potential for biomedical applications.[224] Along with Co doping, HAp was also reported to be substituted with Ce^{3+} or Mg^{2+} using a MW-assisted method. The Ce^{3+} substitution increased the NP size, while Mg^{2+} induced a platelet morphology at 5% substitution. The samples exhibited no cytotoxicity towards bone cells and showed antimicrobial activity, especially against Gram-positive bacteria and *C. albicans*, with Ce^{3+}-substituted HAp demonstrating improved biofilm inhibition, highlighting their potential for bone tissue engineering application.[225] Similarly, scientists also developed a porous chitosan-organically modified montmorillonite-hydroxyapatite (CS-OM-HAp) composite scaffold using MW irradiation and gas foaming. The composite scaffolds exhibited enhanced mechanical and biological properties, including improved swelling (Fig. 8(f-i)) and degradation (Fig. 8(f-ii)) compared to the pure CS scaffolds. The incorporation of HAp and OM into the CS scaffold reduces non-specific protein adsorption by occupying active sites on the HAp surface (Fig. 8(f-iii)), potentially minimizing fibrosis tissue thickness and macrophage adhesion *in vivo*. The CS-OM-HAp scaffold demonstrated non-cytotoxicity toward MG 63 osteoblast cells, underscoring its potential for non-load-bearing bone tissue engineering applications.[226]

The integration of antimicrobial NMs into regenerative medicine has opened new avenues for enhancing tissue repair while preventing infection. In wound healing and tissue engineering, microbial contamination remains a major obstacle that can delay regeneration and compromise clinical outcomes. NMs with inherent or functionalized antimicrobial properties offer a dual advantage; they not only support cellular growth and tissue remodelling but also actively combat pathogenic microorganisms.[214,227] For instance, a simple one-pot MW-assisted hydrothermal method was used to synthesize CDs from citric acid alone. Within just 8 min of irradiation, highly luminescent, photostable, and water-soluble CDs (1.5–4.5 nm) were obtained. These nanostructures showed strong UV absorption and visible emission and proved effective as photosensitizers for antimicrobial photodynamic therapy (aPDT). Under blue LED light (450 nm), they achieved complete eradication of *S. aureus* in both planktonic and biofilm states, with significant bacterial reduction in infected wound models, highlighting their potential as low-cost, efficient agents for aPDT.[227] In another study, another type of water-soluble ZnO@APTES QDs was synthesized using a MW-assisted hydrothermal method, which demonstrated strong antibacterial activity, particularly against methicillin-resistant *S. aureus* (MRSA). These uniformly sized (~5 nm), highly dispersible QDs showed excellent biofilm disruption and inhibition capabilities, with a minimum inhibitory concentration (MIC) of 32 μg mL^{-1} for MRSA. Their mechanism involved membrane binding, ROS generation, and intracellular disruption, ultimately leading to bacterial death without inducing resistance over prolonged exposure, unlike conventional antibiotics. Importantly, the QDs exhibited low cytotoxicity and high biocompatibility, and significantly reduced the bacterial load in a mouse wound infection model. These findings reinforce the growing importance of antimicrobial NMs in regenerative medicine, where preventing infection is critical for successful tissue repair and healing.[214] Building on the growing utility of MW-assisted NMs in antimicrobial applications relevant to regenerative medicine, ZnPc-CDs have emerged as a suitable dual-function phototherapeutic agent. ZnPc-CDs were developed in 2 min *via* the pyrolysis of zinc(II) tetra-amino-phthalocyanine and citric acid. These ~5 nm particles exhibited strong NIR absorption, high water dispersibility, and a positive surface charge for enhanced bacterial targeting. Under dual-laser irradiation (660 nm and 808 nm), they achieved synergistic photodynamic and photothermal antibacterial effects, effectively eradicating *S. aureus* and *E. coli*. Their potent, non-antibiotic antimicrobial action highlights their promise for infection control in regenerative medicine.[228] Another type of carbon NPs (CNPs) was developed by Dechsri *et al.* and applied in antibacterial therapy and infection control through photodynamic therapy (PDT). In this study, MW pyrolysis of gallic acid at 200 °C for 20 min yielded gallic acid-derived CNPs (GACNPs) with a uniform size, negative surface charge, and high thermal stability. These GACNPs exhibited potent antibacterial activity against *S. aureus* and *E. coli* (MIC ~0.29 mg mL^{-1}), which was significantly enhanced under visible light *via* photodynamic effects. When incorporated into PVA-based hydrogels, GACNPs retained their antimicrobial efficacy and outperformed commercial Ag-hydrogel dressings, offering improved mechanical strength, water absorption, and stability. These results highlight GACNPs as favorable candidates for light-activated antimicrobial wound dressings in regenerative medicine.[229] In a recent work, a short-term MAS approach has been adopted to synthesize Baghdadite ($Ca_3ZrSi_2O_9$) NPs, which demonstrated good bioactivity, bio-

compatibility, and enhanced potentiality towards its application for bone regeneration.[230]

MW-assisted synthesis offers a rapid, energy-efficient approach for developing nanostructures with tailored properties for tissue engineering. However, despite the promising advances, several limitations of MAS must be considered. Firstly, the long-term toxicity and immune responses of the NMs prepared *via* MAS remain poorly understood, particularly for metals such as silver and cobalt-doped HAp. Secondly, the biodistribution and clearance of nanoparticles *in vivo* can lead to unintended deposits in organs such as the liver, spleen, and kidneys, raising safety concerns. Thirdly, the reproducibility and scalability of MW-assisted synthesis may be challenging when moving from the lab to clinical-grade production. Finally, regulatory approval for clinical translation requires extensive safety and efficacy studies, which are currently limited for many novel NMs. Thus, future research should focus on optimizing MW parameters, integrating green synthesis strategies, and exploring multifunctional nanostructures for enhanced regenerative outcomes.

4.2. Microwave-assisted nanostructures in biosensing and imaging

MW-assisted synthesis has revolutionized the development of nanostructures specifically tailored for biosensing applications.[231,232] This innovative technique facilitates the rapid and uniform heating of precursors, enabling the synthesis of highly uniform and functional nanostructures with exceptional reproducibility. In biosensing, the precise control over nanostructure size, morphology, and surface chemistry achieved through MW-assisted methods translates to enhanced sensor performance, including higher sensitivity, faster response times, and lower detection limits.[233] Moreover, this approach can produce nanostructures with superior catalytic, optical, and electronic properties, ensuring improved signal transduction and selectivity in detecting biological analytes such as proteins, nucleic acids, and small molecules,[81,234–236] The efficiency and scalability of MW-assisted synthesis further make it a practical choice for integrating advanced NMs into biosensors, advancing the development of reliable, cost-effective, and point-of-care diagnostic tools.

In this context, several intriguing reports highlight DNA-functionalized AuNPs synthesized *via* MW-assisted methods for cell imaging, as shown in Fig. 9(a).[235] Most biosensing applications focus on the electrochemical and optical detection of various biomarkers, including glucose,[177,237,238] dopamine,[239] and alkaline phosphatase.[240] For example, hybrid transition metal-based compounds have shown excellent performances in enzyme-free glucose sensing.[241] A MW-assisted strategy was used to synthesize bimetallic Co/Zn metal–organic frameworks (ZIF67/ZIF8), with structural characterization confirming the optimized Co/Zn ratios, as evident in Fig. 9(b). This synergy enhanced the glucose sensing, achieving a sensitivity of 833.61 μA mM^{-1} cm^{-2}, a wide linear range up to 5 mM, and a detection limit of 6.5 μM. Real-time human serum analysis demonstrated strong anti-interference and recovery rates. This low-cost, eco-friendly method provides an optimistic approach for non-enzymatic glucose detection. Another report also involved the fabrication of a wearable non-enzymatic glucose sensor (Fig. 9(c)), which was developed by synthesizing ternary nickel–cobalt sulfide nanostructures (Ni–Co–S NSs) on commercial fabrics (CFs) using a one-step MW-assisted method.[242] The sensors demonstrated two linear detection ranges (0.04–2.3 mM and 2.31–9.91 mM), sensitivities of 628.1 and 242.8 μA mM^{-1} cm^{-2}, and a low detection limit of 28.7 μM. They exhibited high selectivity, repeatability, and long-term stability. The glucose levels in human serum were accurately measured, confirming the potential of Ni–Co–S@CFs as flexible, foldable platforms for wearable glucose sensing. Another glucose sensor was reported by Savariraj *et al.* for the non-enzymatic detection of glucose from urine samples.[243] The reported bismuth selenide (Bi_2Se_3)-modified glass carbon (GC) electrode exhibited a low detection limit of 6.1 μM, a linear range of 10 μM to 100 μM, and excellent stability, remaining 83% effective after 19 days. In addition, it effectively detected glucose in the presence of other biomarkers such as uric acid (UA), ascorbic acid (AA), dopamine (DA), and sucrose (Fig. 9(d)). These impressive electrocatalytic properties were attributed to the MW-assisted synthesis of three-dimensional Bi_2Se_3 nanostructures, exfoliated into few layers, which enhanced the performance of the sensor for non-enzymatic glucose detection. Along with glucose, glutathione (GSH) is a crucial biomarker for oxidative stress, playing a key role in protecting cells from damage. Abnormal GSH levels are linked to diseases such as cancer and neurodegenerative disorders. Detecting GSH is vital for early diagnosis, monitoring disease progression, and evaluating antioxidant therapies.[244] In this regard, a fluorescent nanosensor was developed for the detection of GSH by Sohal *et al.* using MW-synthesized CDs and hydrothermally prepared MnO_2 nanostructures (nanoflowers, nanorods, and mixtures). The morphology of MnO_2 influenced the photophysical properties of CDs, affecting the fluorescence quenching and electron transfer rates. The best fluorescence recovery upon the addition of GSH was achieved with nanoflowers, yielding a detection limit of 19 μM for GSH (Fig. 9(e)i–iv). The sensing probes were rapid, cost-effective, and eco-friendly for GSH detection. Alkaline phosphatase (ALP) is an important biomarker for diagnosing and monitoring various health conditions, including liver and bone disorders, cancers, and cardiovascular diseases.[245] To detect ALP, fluorescent silver coordination polymer NPs were synthesized *via* a MW-assisted method using terephthalic acid and silver nitrate (Fig. 9(f)i).[240] In this case, a fluorescent "turn-off" method was developed to detect ALP activity, where ALP catalyzed the hydrolysis of ascorbic acid 2-phosphate (AA2P) to ascorbic acid (AA), triggering fluorescence quenching through the reduction of Ag^+ to silver NPs. This method demonstrated high selectivity towards ALP compared to others (Fig. 9(f)ii), a linear detection range (0.2–12 mU mL^{-1}, r = 0.991), and a low detection limit (0.07 mU mL^{-1}). In serum analysis, recoveries of 99.5%-101.2% and RSDs below 4% highlighted its accuracy and

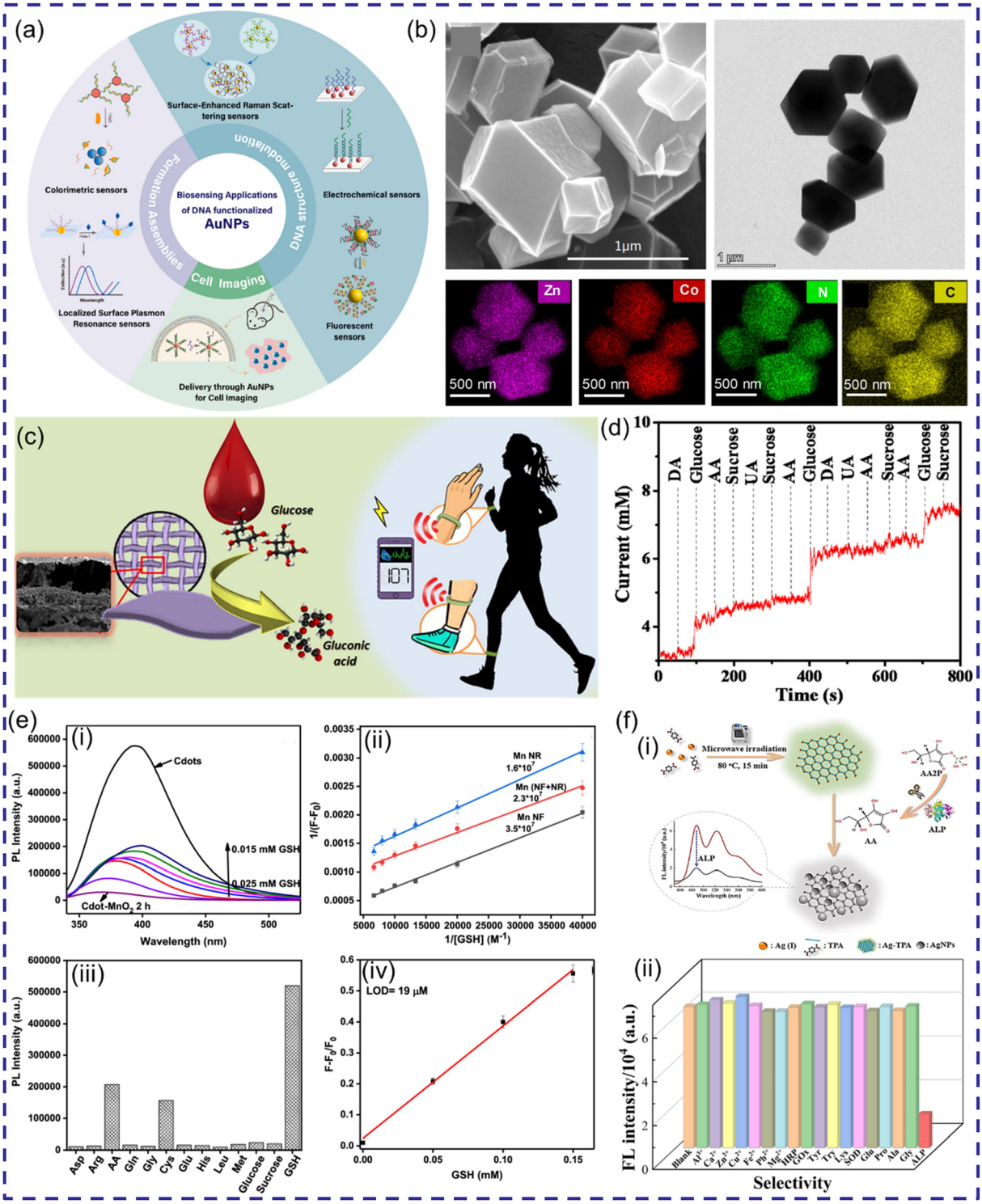

Fig. 9 (a) Applications of DNA-functionalized AuNPs synthesized *via* MW-assisted methods.[235] (b) SEM and TEM images and elemental mapping of Co/Zn metal–organic frameworks (ZIF67/ZIF8).[241] (c) Schematic of ternary nickel-cobalt sulfide nanostructure (Ni–Co–S NS)-based wearable sensor for glucose detection.[242] (d) Glucose detection ability of bismuth selenide (Bi_2Se_3)-modified glass carbon (GC) electrodes.[243] (e) (i–iv) Fluorometric response from the CD/MnO_2 nanostructure-based nanosensor with varying concentrations of GSH.[245] (f) (i) Synthesis of silver coordination polymer NPs and their (ii) ALP detection ability.[240] (a) Reproduced with permission from ref. 235 with permission from Elsevier, Copyright 2024, (b) reproduced with permission from ref. 241 with permission from Elsevier, Copyright 2022, (c) reproduced with permission from ref. 242 with permission from Elsevier, Copyright 2021, (d) reproduced with permission from ref. 243 with permission from Elsevier, Copyright 2020, (e) reproduced with permission from ref. 245 with permission from Springer, Copyright 2023, and (f) reproduced with permission from ref. 240 with permission from MDPI, Copyright 2023.

reliability for ALP detection. Another interesting report Sun *et al.* showed the effective detection of AA, DA, and UA.[246] In this study, graphene oxide nanoribbons (GONRs) were synthesized *via* MW-assisted unzipping of multiwalled carbon nanotubes (MWCNTs) and used to modify glassy carbon (GC) electrodes. The MWCNT/GONR/GC electrode demonstrated a superior electrochemical performance for the simultaneous detection of AA, DA, and UA with well-separated voltammetric peaks and enhanced peak currents. The excellent performance was attributed to the unique electronic structure and enriched oxygen functionalities of MWCNTs/GONRs. Similarly, there is another report on the detection of DA in urine.[239] In this work, silver–chitosan (CS) NPs (Ag-CS NPs) were synthesized *via* MW-assisted green methods, which exhibited antioxidant activity (IC_{50}: 36.94 μg mL^{-1}), antibacterial effects, and effective detection of DA in urine with a limit of detection (LOD) of 0.01 μM and a μM linear range of 0.1–60. Along with the aforementioned biomarkers, detecting other biomarkers such as acetylcholinesterase is vital for monitoring neurodegenerative diseases, while bisphenol A (BPA) detection is essential due to its endocrine-disrupting effects and associated health risks, including hormonal imbalances. For instance, MW-assisted nanostructures have been reported for detecting these specialized biomarkers such as Cu_2O nanospheres with laccase-like nanozyme activity were synthesized *via* a one-pot MW-assisted method.[247] The nanozyme allowed the naked-eye detection of acetylcholinesterase with a sensitivity of 2.5 pM, offering a robust, recyclable platform for biosensing. For the detection of BPA, polyaniline-bismuth oxybromide (PANI-BiOBr) nanocomposites were synthesized *via* a MW-assisted green synthesis approach.[248] The developed nanocomposite exhibited enhanced conductivity, high sensitivity, a low detection limit (0.19×10^{-9} μM), and a wide linear range (0.19×10^{-9} to 3.04×10^{-3} μM). It demonstrated excellent selectivity, stability, and reproducibility, effectively detecting BPA in real samples and showing promise for broader applications in identifying estrogenic compounds.

MW-assisted methods have also emerged as powerful tools for developing NMs with tailored magnetic and optical properties for biomedical imaging. For instance, citrate-coated superparamagnetic iron oxide NPs (SPIONs) were synthesized *via* MW irradiation (96–110 °C) using iron salts and citric acid, resulting in monodisperse, water-soluble particles. These SPIONs exhibited superparamagnetic behaviour, high transverse reflexivity, and strong MRI contrast comparable to commercial agents. They were efficiently internalized by human mesenchymal stromal cells with minimal cytotoxicity, demonstrating excellent potential for the non-invasive monitoring of tissue regeneration.[249] Alternatively, MW-assisted synthesis has been extended to green NMs such as CDs, which have been widely used as contrast agents for bioimaging[250,251] For example, CDs were produced from *Calotropis gigantea* leaf extract *via* a one-step MW carbonization method. The resulting ~5.7 nm CQDs demonstrated multi-colour fluorescence, excellent water solubility, and photostability. They effectively labelled bacteria, fungi, and plant cells at low concentrations, highlighting their promise for eco-friendly and biocompatible imaging applications.[252] Another report highlights the utility of plant-derived NMs, where the MW-assisted synthesis of CDs from *Plectranthus amboinicus* leaves produced ~2.4 nm crystalline CDs with excellent photoluminescence and water solubility. These CDs exhibited low cytotoxicity and enabled the effective bioimaging in MCF-7 cells, underscoring their potential for biosensing and diagnostic applications.[253]

MW-assisted synthesis enables the rapid, eco-friendly production of nanostructures with enhanced biosensing and imaging capabilities. Although MW-assisted nanostructures offer enhanced sensitivity and selectivity for biosensing and imaging, their toxicity and biocompatibility remain critical concerns, especially for *in vivo* applications. Many fluorescent or metallic nanoparticles may generate ROS or interfere with normal cellular processes if internalized, but these studies have not yet been accomplished. Also, their biodistribution and clearance profiles are often poorly characterized, which can limit their use in repeated imaging or long-term monitoring. Furthermore, standardization and reproducibility across different synthesis batches are challenging due to variations in MW conditions and precursor materials. Finally, integration into regulatory-compliant diagnostic platforms requires rigorous validation, which is not yet widely reported. Thus, addressing these issues is key to advancing the clinical applications of MW-assisted nanostructures.

4.3. Microwave-assisted nanostructures in cancer therapy

MW-assisted nanostructures have emerged as encouraging tools in cancer therapy due to their rapid synthesis, tunable properties, and eco-friendly production. These nanostructures enable precise drug delivery, imaging, and thermal ablation, addressing challenges in targeted cancer treatments.[254] Recent studies focus on developing multifunctional nanoplatforms for simultaneous drug delivery and photothermal therapy, as well as enhancing imaging-guided treatment strategies.[255–257] These advancements pave the way for efficient, minimally invasive, and cost-effective cancer therapeutic approaches.

For instance, recently, a new molybdenum and [2,2′-bipyridine]-4,4′-dicarboxylic acid (Mo/BPDA) nanocomposite was synthesized and evaluated for ITS anticancer activity.[258] The nanocomposite demonstrated significant anticancer effects against bone and breast cancer cells, with cell proliferation and viability ranging from 37.36% to 82.07% that of the control, and an IC_{50} value between 33 and 43 μg mL^{-1} after 24 and 48 h of treatment. These results suggest that the Mo/BPDA nanocomposite could be a promising candidate for cancer therapy. Photothermal therapy offers a selective and minimally invasive approach for cancer treatment, overcoming the drawbacks of traditional therapies.[259] Polypyrrole (PPy) NPs, with excellent photothermal properties and biocompatibility, show promise in tumor ablation and various biomedical applications.[260] A MW-assisted method has been developed to rapidly synthesize PPy NPs in 2 min, enhancing their photothermal performance and reducing their synthesis time.[260] This method enables effective *in vivo* tumor ablation under

safe laser irradiation, showcasing the potential of PPy NPs in cancer therapy and other biomedical fields (Fig. 10(a)i and ii).[260] In another study, ZnO NPs were synthesized *via* a MW-assisted green method using *Pistia stratiotes* leaf extract, resulting in 35 nm particles with a spherical structure (Fig. 10(b) i).[159] The ZnO NPs exhibited significant anticancer activity against SK-MEL-28 melanoma cells (Fig. 10(b)ii), with an IC_{50} value of 51.05 μg mL^{-1}. In contrast to ZnO, Ag NPs and Au NPs were biosynthesized using *Borassus flabellifer* fruit extract under MW irradiation, resulting in spherical NPs with sizes of 7–9 nm and 5–7 nm, respectively.[261] These NPs also exhibited anticancer properties against MCF-7 breast cancer cells, suggesting their potential applications in cancer therapy. Ag NPs were also synthesized using *Coriolus versicolor* and *Boletus edulis* mushroom extracts *via* MW-assisted green synthesis.[150] The resulting nanoparticles exhibited strong anticancer, antibacterial, antifungal, and wound healing activities, highlighting their potential for biomedical applications.

In a recent report, MW-synthesized pH-sensitive CNPs offered a fast, efficient drug delivery system for doxorubicin (DOX) in cancer treatment. With a high drug-loading (85.82%), these NPs enabled controlled, tumor-targeted release, enhancing the efficacy of DOX, while minimizing its toxicity. CNPs-DOX demonstrated superior anticancer activity, inducing apoptosis in MDA-MB-231 cells. Their biocompatibility, nanoscale size (~43.2 nm), and rapid synthesis make them capable of cancer therapy.[256] Additionally, MW-assisted synthesized NMs have also been utilized for PTT in cancer treatment. For example, MW-assisted GdB_6 NPs offered a novel photo-theragnostic approach for cancer treatment, combining fluorescence imaging and NIR-PTT. Their bright greenish-yellow fluorescence enabled precise cell tracking, while their high NIR absorption ensures efficient photothermal tumor ablation. *In vitro* and *in vivo* results confirmed superior antitumor efficacy and biocompatibility, making GdB_6 NPs a suitable multifunctional nanoplatform for precision oncology.[262] In another study, MW-synthesized MIL-100(Fe) NPs enabled combined chemo-photothermal therapy for colorectal cancer by co-delivering oxaliplatin and indocyanine green. These NPs offered a high drug-loading, precise imaging, and targeted treatment, while inducing immunogenic cell death and enhancing the immune response, highlighting their potential as a propitious nanoplatform for advanced colorectal cancer therapy.[263] Building on this, MW-assisted synthesis has also enabled the development of NIR-active CDs for photothermal cancer therapy. Using citric acid with either urea or ammonium fluoride in a one-pot MW-assisted hydrothermal method, CDs with strong NIR absorbance and photothermal conversion were produced. Notably, MF-derived CDs showed superior heating (~46 °C at 1250 μg mL^{-1} in 5 min under 808 nm laser) and effectively ablated HeLa and MCF7 cells *in vitro* and *in vivo*, demonstrating potent tumor suppression with minimal toxicity.[264]

In addition to PTT, PDT has emerged as an effective and minimally invasive strategy for eliminating tumor cells

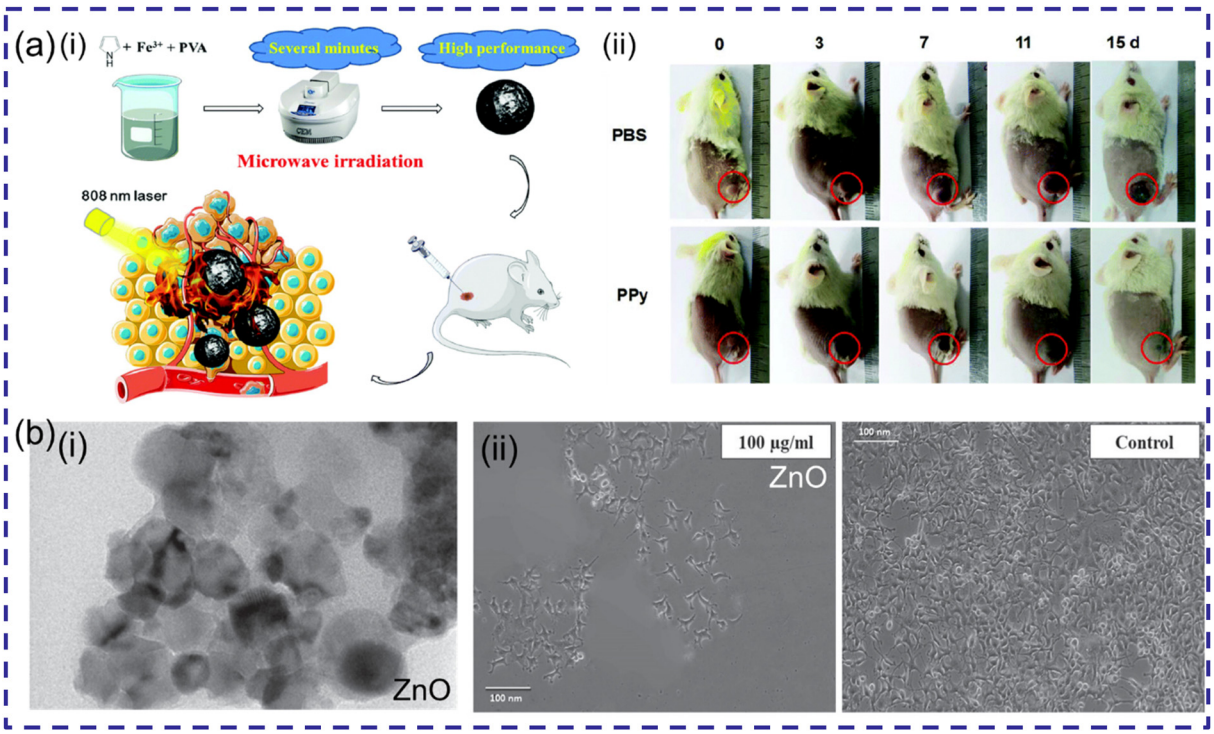

Fig. 10 (a) (i) MW synthesis of PPy NPs and schematic of their anti-tumor activity. (ii) *In vivo* anti-tumor activity of the developed PPy NPs in a rat model.[260] (b) (i) Spherical structure of ZnO NPs. (ii) *In vitro* anticancer activity against SK-MEL-28 melanoma cells.[159] (a) Reproduced from ref. 260 with permission from The Royal Society of Chemistry, Copyright 2018 and (b) reproduced from ref. 159 with permission from IOP publishers, Copyright 2024.

Table 4 Applications of the MW-assisted fabrication of different NMs and nanostructures in biomedicine

Sl. no.	Nanomaterials	Shape/size (nm)	Approach	Application	Ref.
1	PdNPs supported by *Limonia acidissima* Groff tree extract gum	Spherical (7–9)	MW-assisted synthesis with tree extract gum	Colorimetric detection of H_2O_2 and glucose	151
2	Cobalt-doped mesoporous hydroxyapatite (Co-HAp) nanorods	Nanorods (2–4 nm thickness and 10–25 long)	MW-assisted synthesis, using black Scallop seashell as a calcium source, oxalic acid as chelating agent	MRI, drug targeting, hyperthermia, cancer treatment, healthcare applications	224
3	Hydroxyapatite (HAp), HAp-Ce, HAp-Mg NPs	Monodisperse, fine NPs (~50)	Hydrothermal maturation in the MW field	Bone grafts, biomaterials for hard tissue implants, and antimicrobial coatings to reduce device-associated infections	225
4	Chitosan–organically modified montmorillonite–hydroxyapatite(CS–OM–HA) Composite	Nanocomposite	MW irradiation and gas foaming method	Non-load-bearing bone tissue engineering applications	226
5	rGO/NiO nanocomposite	NiO (rod-shaped) distributed on the rGO nanosheets	MW-assisted hydrothermal method (with and without organic/reducing agents and subcritical water)	Non-enzymatic glucose detection	237
6	Silver–chitosan NPs	Nanosphere (19–49)	MW-assisted green synthesis (80–120 °C)	Dopamine sensing from urine	239
7	Fluorescent silvercoordination polymer NPs	Nanoparticles (200)	Ultra-rapid MW-assisted strategy	Fluorescent detection of alkaline phosphatase activity	240
8	Co/Zn metal–organic frameworks (ZIF67/ZIF8)	Rhomboid dodecahedral structure (~400)	MW-assisted one-step green strategy for bimetallic framework synthesis	Non-enzymatic glucose sensing with high sensitivity and wide linear range	241
9	Ni–Co–S nanostructures on commercial fabrics (Ni–Co–S@CFs)	Nanostructures on CFs	One-step MW-assisted synthesis	Wearable non-enzymatic glucose sensing	242
10	Graphene oxide nanoribbons	Nanoribbons	MW-assisted unzipping of multiwalled carbon nanotubes	Electrochemical detection of ascorbic acid, dopamine, and uric acid	246
11	Cu_2O	Nanospheres (500–1000)	One-pot polyol-based MW-assisted method	Phenolic oxidation, acetylcholinesterase sensing	247
12	Polyaniline (PANI)-bismuth oxybromide nanocomposite	Globular deposition on PANI	MW-assisted green synthesis	Electrochemical detection of endocrine disruptor bisphenol-A	248
13	Polypyrrole (PPy) NPs	Nanospheres (50 and 70)	MW-assisted synthesis (2 min)	Photothermal therapy for tumor ablation, biosensing, electrochemical sensors, tissue engineering, and flexible microelectronics	260
14	DNA-functionalized AuNPs	Nanosphere (5–100)	MW synthesis, shielding charge repulsion, and DNA customization	Biosensing applications	266
15	Carbon dots@MnO_2	Nanoflowers, nanorods, and their mixture	MW-assisted pyrolysis (carbon dots) and hydrothermal (MnO_2)	Fluorescent detection of glutathione	267
16	Ni@NSiC-900 biomass nanocomposite	Nickel NPs wrapped by an ultra-thin carbon shell (~3)	MW-assisted synthesis of $NiSiO_3$/CNx, ammonia etching at 900 °C	Glucose biosensor with high sensitivity and selectivity	268
17	Bismuth selenide (Bi_2Se_3) few layers (Bi_2Se_3-FL)	Few-layered nanostructures	MW-assisted synthesis using water as solvent and hydrazine hydrate as reducing agent	Non-enzymatic glucose sensing	269
18	Silver and gold NPs	Spherical (~7–9 for AgNPs, ~5–7 for AuNPs)	MW-assisted biosynthesis using *Borassus flabellifer* fruit extract	Antibacterial/anticancer applications	270
19	Molybdenum-bipyridine dicarboxylic acid (Mo/BPDA) nanocomposite	Nanocrystals with octahedral morphology (~5–10)	MW-assisted synthesis	Antibacterial, antifungal, and anticancer properties, with potential applications in treating infectious diseases and cancer	258
20	Copper oxide (CuO) NPs	Nanoparticles (~30)	MW-assisted biogenic synthesis using *Andrographis paniculata* extract	Antibacterial and anticancer activity (A549: IC50: 14.76 μg mL^{-1})	271
21	Zinc oxide (ZnO) NPs	Spherical, flower and sheet (~35)	MW-assisted green synthesis using *Pistia stratiotes* leaf extract	Antibacterial, antifungal, and anticancer therapies (IC50: 51.05 μg mL^{-1} against melanoma)	272

Table 4 *(Contd.)*

Sl. no.	Nanomaterials	Shape/size (nm)	Approach	Application	Ref.
22	Multi-substituted hydroxyapatite (SHA) nanopowder	Spherical particle (50–90)	MW-assisted synthesis	Implant coating, bone tissue engineering, orthopaedic applications	273
23	ZnO NPs	Spherical (70–90)	MW-assisted method using ascorbic acid and PVA as a capping agent and stabilizing agent	Antimicrobial activity against *Salmonella typhi*, *Klebsiella* spp., *E. coli*, and *S. aureus*	274
24	Gold-loaded hydroxyapatite with collagen coating	Nanoparticles (24 ± 6)	MW-assisted synthesis, wet precipitation for HAp, Au loading, and collagen coating	Drug delivery (DOX), scaffold materials for biomedical applications, bone tissue engineering, and regenerative medicine	275
25	*Aloe vera* extract- coated metallocene polyethylene (mPE)	Nanoscale roughness on mPE surface	MW-assisted coating of *Aloe vera* extract on mPE	Multifaceted biomedical implants for tissue engineering	276

through light-activated reactive oxygen species (ROS) generation. Recent advances in MW-assisted synthesis have enabled the development of photodynamically active NMs with enhanced efficacy and selectivity. For instance, Murali *et al.* synthesized hematoporphyrin-derived carbon quantum dots (HP-CDs) *via* a one-step, 5 min MW-assisted reaction using hematoporphyrin and tris(2-aminoethyl) amine in Tris buffer. The resulting ~9 nm particles exhibited strong red-light absorption, a positive surface charge (+24.3 mV), and excellent water solubility. Upon 635 nm irradiation, HP-CQDs generated a high yield of singlet oxygen ($\phi \approx 0.42$), demonstrating superior phototoxicity and lower dark toxicity against MCF-7 breast cancer cells compared to free hematoporphyrin. Their stable dispersion, efficient cellular uptake, and effective PDT-mediated cell killing underscore the potential of MW-synthesized nanostructures for targeted cancer therapy and microbial control.[257]

In conclusion, MW-assisted nanostructures have shown significant potential in revolutionizing cancer therapy by enhancing drug delivery, improving targeting precision, and minimizing the invasiveness of traditional treatments. However, despite their encouraging results in photothermal, photodynamic, and drug delivery applications, several limitations remain. The toxicity and off-target effects of nanostructures, particularly metal-based or carbon-based particles, have not been fully elucidated *in vivo*. Their biodistribution and retention in tumors *versus* healthy tissues can be unpredictable, potentially leading to systemic toxicity. Thus far, it has been reported that particles or nanostructures with dimensions below 10 nm can undergo renal clearance from the body;[265] however, the clearance pathways for larger particles remain less well understood. Larger nanostructures may accumulate in the liver, spleen, or reticuloendothelial system, leading to prolonged retention and potential toxicity. Therefore, understanding the size-dependent biodistribution and clearance mechanisms is essential for designing safe and clinically translatable NMs. Challenges also exist in scaling up the synthesis of NMs, while maintaining their precise size, shape, and functionalization, which is critical for reproducibility and clinical translation. As research continues to advance, the integration of MW-assisted nanostructures could pave the way for highly efficient, personalized cancer therapies with broad clinical applications, offering substantial promise for future medical breakthroughs.

A comprehensive summary of the different applications of the MAS of NMs in the field of biomedicine is presented in Table 4.

4.4. Other miscellaneous biomedical applications

Beyond the well-established roles of nanostructures in cancer therapy, bioimaging, biosensing, tissue engineering, and infection control, MW-assisted NMs have demonstrated significant potential across a diverse array of additional biomedical applications. These applications include drug delivery, vaccine development, and gene therapy.[277–281] This section highlights the recent advances in these miscellaneous applications, underscoring the versatility and expanding impact of MW-fabricated nanostructures in biomedicine.

In a recent report, MW-assisted synthesis has also enabled the development of multifunctional superabsorbent agar-based magnetic hydrogels (AMHs) *via* the free radical polymerization of acrylic acid, acrylamide, and AMPS in the presence of iron oxide NPs. The resulting hydrogels exhibited high elasticity, swelling capacity (up to 11 720%), and magnetic responsiveness. The ciprofloxacin-loaded AMHs demonstrated efficient drug encapsulation (up to 120 mg g^{-1}) and sustained release (~80%) in 24 h. *In vivo* studies confirmed their low dermal toxicity, anti-inflammatory effects, and accelerated wound healing, highlighting their potential for controlled drug delivery and regenerative medicine applications.[282] Building on the versatility of MW-fabricated drug delivery platforms, a study demonstrated the MW-assisted synthesis of mesoporous hydroxyapatite (MHA) NPs using calcium nitrate, ammonium phosphate, and CTAB as a template. The rapid MW process yielded uniform rod-shaped MHA particles with mesopores, exhibiting a high surface area and enhanced pore volume. These features enabled efficient atorvastatin loading (~85%) and sustained release in PBS. *In vitro* results showed

their excellent cytocompatibility with MG-63 osteoblast-like cells and enhanced mineralization, suggesting their strong potential for periodontal bone regeneration.[283] From a vaccine delivery perspective, an interesting report described a MW-assisted method for the rapid synthesis of lipid NPs (LNPs), including non-ionic surfactant vesicles and bilosomes, by irradiating lipid mixtures at 140 °C for 2 min in carbonate buffer. Tetanus toxoid (TT) was efficiently encapsulated, with bilosomes achieving ~31% entrapment efficiency. Upon oral or nasal administration in mice, the TT-loaded bilosomes, especially those containing xanthan gum, elicited strong systemic I_gG responses and provided 100% protection against toxin challenge, highlighting the potential of this platform for mucosal, needle-free vaccine delivery.[284]

In summary, MW-assisted synthesis offers a rapid, efficient, and versatile approach for fabricating diverse nanostructures for biomedical applications, including drug delivery and vaccine platforms. However, although MW-assisted NMs show promise for drug delivery, vaccine platforms, and gene therapy, important limitations remain. The toxicity and immune responses to nanoparticles, especially after repeated administration, require thorough evaluation, which has yet to be reported. Also, their biodistribution and pharmacokinetics are often unclear, which could affect their therapeutic efficacy and safety. Finally, translating these platforms to clinical use demands comprehensive studies addressing their long-term stability, biocompatibility, and regulatory compliance, which are currently limited in the present literature.

5. Conclusion and future prospects

Innovation and research in the field of materials science have opened new perspectives in every field of science and technology, which in turn have urged researchers to explore new synthetic routes. Considerable efforts are committed to achieving minimized energy consumption and sustainable chemical processing, as researchers are constantly urged to adopt more environmentally friendly fabrication methods. MAS has been widely explored as a rapid and cost-effective methodology to fabricate a wide range of NMs. Central to MAS is the regulation of the power, irradiation time, frequency, and choice of solvents. These characteristics affect the size and morphology of the fabricated NMs. Compared to the conventional fabrication routes for NMs, MAS has many advantages, including higher heating rates, no direct contact between the chemical reaction mixture and the energy source, rapid reaction rate, and high yield, which illuminate the critical role of MAS in the field of material fabrication. However, despite the significant progress in these MAS approaches, they suffer from several disadvantages, which further restrict their commercialization.

1. Proper understanding of the heating mechanism: The heating processes in MAS approaches are completely different from the conventional processes. However, the understanding of the exact heating mechanism has not been established to date. Although a few heating mechanisms have been proposed in this aspect, they suffer from a lack of appropriate evidence. Therefore, to improve the quality and product yield, a proper understanding of the MW heating mechanism with theoretical simulation is highly essential.

2. Designing of appropriate MW reactor: For commercialization, the scaling up of the MW reactor is considered a critical issue. To apply effective and uniform heating through MW irradiation, the construction of commercial MW reactors should focus on several factors, including the geometry of the reactor, effective power coupling, and proper control of the reaction temperature. In this aspect, the modern single-mode reactors can be considered to overcome the issue of uniform heating by exactly controlling the MW field. The single-mode reactors excite a unique single electromagnetic mode, which enables them to produce a controllable and reproducible heating environment.

3. Limitations in selecting materials: The product quality of MAS approaches is highly dependent on the compatibility of the precursor materials with MW. It is evident that usually, non-conductive materials do not absorb MW efficiently. Notably, this limitation of MAS approaches affects the mass production of a wide range of materials for their applications in various fields. In this aspect, advanced MW-assisted approaches with selective materials should be designed to enhance the scalability. Future research should be directed towards the MAS of mesoporous and core–shell structured high-entropy NPs. Furthermore, special attention should be paid to developing chiral nanostructures with controlled enantioselectivity using MAS approaches.

4. Issue of uniform heating in MAS processes for commercialization: The penetration depth of MWs is found to be limited. This low penetration depth affects the uniform heating of materials, specifically on larger scales. Consequently, the uneven heating in MAS approaches significantly deteriorates the quality of the MW-synthesized products. In this aspect, a proper understanding of the MW heating mechanism and exploring advanced MW apparatus with a larger penetration depth is highly essential.

5. Competition with conventional approaches: It is evident that MAS approaches are beneficial compared to the conventional heating approaches in terms of shortening the reaction time. However, the large-scale production of materials also depends on other factors. In this aspect, MAS approaches suffer from high maintenance costs, a lack of expertise, high installation costs on a large scale, expensive operating costs, improper control over morphologies, *etc*. In comparison, the conventional heating approaches are found to be cheaper than MAS approaches on large scales.

6. Scale-up challenges in industrial or clinical translation: The penetration depth of microwaves is subject to MW irradiation frequency, and thus a lower penetration depth would imply non-uniform heating, and thus a relatively hotter outer surface, while the inner solution mixture would heat gradually *via* convection currents. Consequently, this would

lead to a lower product yield or morphological imperfections, which is crucial for implication in MAS-enabled nanoparticle synthesis in a clinical or industrial setup. Moreover, localised hotspots also pose significant scale-up challenges. In addition to the aforementioned heating challenges, designing large-scale industrial MW setups requires high costs and engineering expertise to avoid uneven heating, sensor malfunctions, and reproducible outcomes. Overall, the setup of MW synthesizers would require expensive infrastructure, highly skilled labour, and a great magnitude of optimisation, before they finally replace conventional synthesis methods in real-world scenarios.

Despite these challenges, expansions in material fabrication through MW irradiation present an optimistic outlook for nanomaterial fabrication and their potential applications in the healthcare sector. Additionally, in the current scenario, MAS has not been explored to its full potential in the field of biomedicine, but it has full potential for future development. Overcoming the limitations of the existing MAS and a comprehensive knowledge of its governing parameters could provide a great platform for designing a wide range of nanostructures and NMs with potential biomedical applications.

Author contributions

Ankur Sood: conceptualization, investigation, formal analysis, writing – original draft. Kanika: investigation, formal analysis, writing – original draft. Arpita Roy: investigation, formal analysis, writing – original draft. Shubham Mahajan: formal analysis, writing – original draft. Sung Soo Han: writing – review & editing, supervision, fund acquisition. Rehan Khan: writing – review & editing, supervision. Sumanta Sahoo: conceptualization, investigation, formal analysis, writing – review & editing.

Conflicts of interest

The authors declare that they have no known competing financial interests or personal relationships that could have appeared to influence the work reported in this paper.

Data availability

No new data were created or analyzed in this study.

Acknowledgements

This work was supported by the Basic Science Research Program through the National Research Foundation of Korea (NRF), funded by the Ministry of Education (NRF-2022R1l1A1A01071419 and RS-2020-NR049591).

References

1 J. Dolai, K. Mandal and N. R. Jana, *ACS Appl. Nano Mater.*, 2021, **4**, 6471–6496.
2 S. Talebian, T. Rodrigues, J. D. Neves, B. Sarmento, R. Langer and J. Conde, *ACS Nano*, 2021, **15**, 15940–15952.
3 V. Mailänder and K. Landfester, *Biomacromolecules*, 2009, **10**, 2379–2400.
4 S. Behzadi, V. Serpooshan, W. Tao, M. A. Hamaly, M. Y. Alkawareek, E. C. Dreaden, D. Brown, A. M. Alkilany, O. C. Farokhzad and M. Mahmoudi, *Chem. Soc. Rev.*, 2017, **46**, 4218–4244.
5 J. Mosquera, I. García and L. M. Liz-Marzán, *Acc. Chem. Res.*, 2018, **51**, 2305–2313.
6 A. Sood, S. S. Das, R. Singhmar, S. Sahoo, M. Wahajuddin, Z. Naseem, S. Choi, A. Kumar and S. S. Han, *Int. J. Biol. Macromol.*, 2025, **292**, 139174.
7 S. Y. Won, R. Singhmar, S. Sahoo, H. Kim, C. M. Kim, S. M. Choi, A. Sood and S. S. Han, *Colloids Surf., B*, 2025, **245**, 114207.
8 B. Lee, Y. Lee, N. Lee, D. Kim and T. Hyeon, *Nat. Rev. Mater.*, 2025, **10**, 252–267.
9 H. Almeida, G. Traverso, B. Sarmento and J. D. Neves, *Nat. Rev. Bioeng.*, 2024, **2**, 609–625.
10 A. C. Anselmo and S. Mitragotri, *Bioeng. Transl. Med.*, 2019, **4**, e10143.
11 V. L. Colvin, *Nat. Biotechnol.*, 2003, **21**, 1166–1170.
12 Y. Xin, T. Nagata, K. Kato and T. Shirai, *ACS Appl. Nano Mater.*, 2022, **5**, 4305–4315.
13 Y.-J. Zhu and F. Chen, *Chem. Rev.*, 2014, **114**, 6462–6555.
14 C. K. Maity, A. Sood, R. Singhmar, J. H. Choi, A. Milton, S. M. Choi, S. Sahoo and S. S. Han, *J. Alloys Compd.*, 2025, **1014**, 178734.
15 M. B. Gawande, S. N. Shelke, R. Zboril and R. S. Varma, *Acc. Chem. Res.*, 2014, **47**, 1338–1348.
16 S. Sahoo, A. Al Mahmud, A. Sood, G. Dhakal, S. K. Tiwari, S. Zo, H. M. Kim and S. S. Han, *J. Sci.: Adv. Mater. Devices*, 2025, **10**, 100843.
17 S. Sahoo, A. Sood, R. Kumar, A. Milton, S. M. Choi, Y. J. Jo, I. Hussain and S. S. Han, *J. Energy Storage*, 2025, **110**, 115368.
18 A. Sood, S. Choi, S. Han, S. Sahoo and S. S. Han, *Mater. Chem. Front.*, 2025, **9**, 2213–2223.
19 A. J. Khan, L. Gao, A. Numan, S. Khan, I. Hussain, M. Sajjad, S. S. Shah, A. Mateen and G. Zhao, *Crit. Rev. Solid State Mater. Sci.*, 2025, **50**, 515–538.
20 R. Kumar, S. Sahoo, R. Pandey, E. Joanni and R. M. Yadav, *Mater. Sci. Eng., R*, 2024, **161**, 100860.
21 Q. Wu, N. Xia, D. Long, L. Tan, W. Rao, J. Yu, C. Fu, X. Ren, H. Li and L. Gou, *Nano Lett.*, 2019, **19**, 5277–5286.
22 Y. Qiao, Y. Xu, X. Liu, Y. Zheng, B. Li, Y. Han, Z. Li, K. W. K. Yeung, Y. Liang, S. Zhu, Z. Cui and S. Wu, *Nat. Commun.*, 2022, **13**, 2461.
23 J. Sun, W. Wang and Q. Yue, *Materials*, 2016, **9**, 231.

24 M. T. Kubo, É. S. Siguemoto, E. S. Funcia, P. E. Augusto, S. Curet, L. Boillereaux, S. K. Sastry and J. A. Gut, *Curr. Opin. Food Sci.*, 2020, **35**, 36–48.
25 S. Tagliapietra, E. C. Gaudino, K. Martina, A. Barge and G. Cravotto, *Chem. Rec.*, 2019, **19**, 98–117.
26 S. Xu, G. Zhong, C. Chen, M. Zhou, D. J. Kline, R. J. Jacob, H. Xie, S. He, Z. Huang and J. Dai, *Matter*, 2019, **1**, 759–769.
27 M. Henary, C. Kananda, L. Rotolo, B. Savino, E. A. Owens and G. Cravotto, *RSC Adv.*, 2020, **10**, 14170–14197.
28 S. Głowniak, B. Szczęśniak, J. Choma and M. Jaroniec, *Adv. Mater.*, 2021, **33**, 2103477.
29 L. Vivas, C. Manquian, D. P. Catalán, P. Márquez and D. Singh, *Front. Energy Res.*, 2025, **12**, 1–11.
30 H. M. Alkhalidi, U. Zaman, D. Khan, K. ur Rehman, K. I. Omar, M. Alissa, W. Y. Rizg, D. M. Bukhary, E. A. Abdelrahman and M. S. Refat, *J. Mol. Liq.*, 2023, **392**, 123469.
31 P. Z. Fathurrohman, E. S. Kunarti, N. Wijayanti and S. J. Santosa, *Discover Appl. Sci.*, 2024, **6**, 311.
32 P. Durairaj, T. Maruthavanan, S. Manjunathan, S. Subashini, S. L. Rokhum and G. Baskar, *J. Mol. Struct.*, 2024, **1295**, 136650.
33 S. K. Murthy, B. V. Basavaraj and B. Srinivasan, *Mater. Today: Proc.*, 2023, DOI: 10.1016/j.matpr.2022.12.227.
34 Y. M. Pusparizkita, R. A. Faizal, S. A. P. Negara, R. Ismail, J. Jamari and A. P. Bayuseno, *Next Mater.*, 2025, **9**, 100946.
35 I. E. Doicin, M. D. Preda, I. A. Neacsu, V. L. Ene, A. C. Birca, B. S. Vasile and E. Andronescu, *Appl. Sci.*, 2024, **14**, 7854.
36 B. Thokchom, S. M. Bhavi, M. B. Abbigeri, A. K. Shettar and R. B. Yarajarla, *Carbon Lett.*, 2023, **33**, 1057–1071.
37 P. Kadyan, M. Kumar, A. Tufail, A. Ragusa, S. K. Kataria and A. Dubey, *Mater. Adv.*, 2025, **6**, 805–826.
38 R. Singhmar, S. Sahoo, S. Choi, J. H. Choi, A. Sood and S. S. Han, *Eur. Polym. J.*, 2024, **220**, 113462.
39 W. Ahmad and S. Kumar, *Emergent Mater.*, 2024, **7**, 1081–1090.
40 B. S. Aliwarga, K. Muhammad, L. A. Asri and A. Wibowo, *Appl. Sci.*, 2024, **15**, 7693.
41 N. Balighieh, S. F. Kashani-Bozorg, M. Kheradmandfard and M. R. Barati, *J. Mater. Sci.*, 2023, **58**, 17066–17079.
42 S. K. Sridhar, P. D. Bhavani, S. Noothi, L. R. Gajula, P. Goudanavar, B. Gowthami and N. R. Naveen, *Curr. Microwave Chem.*, 2024, **11**, 95–115.
43 S. Kumar, P. Sekar and S. K. Raju, *Adv. Pharm. J.*, 2023, **8**, 1–16.
44 Z. Li, K. Peng, N. Ji, W. Zhang, W. Tian and Z. Gao, *Nanoscale Adv.*, 2025, **7**, 419–432.
45 S. Virlley, S. Shukla, S. Arora, D. Shukla, D. Nagdiya, T. Bajaj, S. Kujur, A. Kumar, J. S. Bhatti and A. Singh, *J. Drug Delivery Sci. Technol.*, 2023, **87**, 104842.
46 N. Kaur, A. Singh and W. Ahmad, *J. Inorg. Organomet. Polym. Mater.*, 2023, **33**, 663–672.
47 H. J. Kitchen, S. R. Vallance, J. L. Kennedy, N. Tapia-Ruiz, L. Carassiti, A. Harrison, A. G. Whittaker, T. D. Drysdale, S. W. Kingman and D. H. Gregory, *Chem. Rev.*, 2014, **114**, 1170–1206.
48 A. Kumar, Y. Kuang, Z. Liang and X. Sun, *Mater. Today Nano*, 2020, **11**, 100076.
49 R. Kumar, S. Sahoo, E. Joanni and R. K. Singh, *J. Energy Chem.*, 2022, **74**, 252–282.
50 N. Devi, S. Sahoo, R. Kumar and R. K. Singh, *Nanoscale*, 2021, **13**, 11679–11711.
51 S. Chahal, S. M. Kauzlarich and P. Kumar, *ACS Mater. Lett.*, 2021, **3**, 631–640.
52 R. Kumar, S. Sahoo, E. Joanni, R. K. Singh and K. K. Kar, *ACS Appl. Mater. Interfaces*, 2021, **14**, 20306–20325.
53 S. Zhang, Q. Qiu, C. Zeng, K.-W. Paik, P. He and S. Zhang, *J. Manuf. Process.*, 2024, **116**, 176–191.
54 J. Robinson, E. Binner, D. B. Vallejo, N. D. Perez, K. Al Mughairi, J. Ryan, B. Shepherd, M. Adam, V. Budarin and J. Fan, *Chem. Eng. J.*, 2022, **430**, 132975.
55 Y. Feng, Y. Tao, Q. Meng, J. Qu, S. Ma, S. Han and Y. Zhang, *Chem. Eng. J.*, 2022, **441**, 135924.
56 J. Lin, S. Sun, D. Xu, C. Cui, R. Ma, J. Luo, L. Fang and H. Li, *Chem. Eng. J.*, 2022, **429**, 132195.
57 D. Xin-Hui, C. Srinivasakannan, P. Jin-Hui, Z. Li-Bo and Z. Zheng-Yong, *Biomass Bioenergy*, 2011, **35**, 3920–3926.
58 T. A. T. Dao, H. K. Webb and F. Malherbe, *Food Hydrocolloids*, 2021, **113**, 106475.
59 N. Dahal, S. Garcia, J. Zhou and S. M. Humphrey, *ACS Nano*, 2012, **6**, 9433–9446.
60 R. Krishnan, D. Agrawal and T. Dobbins, *J. Alloys Compd.*, 2009, **470**, 250–255.
61 N. Wang, W. Zou, X. Li, Y. Liang and P. Wang, *RSC Adv.*, 2022, **12**, 17158–17181.
62 A. De la Hoz, A. Diaz-Ortiz and A. Moreno, *Chem. Soc. Rev.*, 2005, **34**, 164–178.
63 A. d. la Hoz, A. Díaz-Ortiz and A. Moreno, *J. Microw. Power Electromagn. Energy*, 2006, **41**, 45–66.
64 G. He, Z. Yan, X. Ma, H. Meng, P. K. Shen and C. Wang, *Nanoscale*, 2011, **3**, 3578–3582.
65 D. Dallinger and C. O. Kappe, *Chem. Rev.*, 2007, **107**, 2563–2591.
66 R. Yathisha and Y. A. Nayaka, *Inorg. Chem. Commun.*, 2020, **115**, 107877.
67 S. K. Seol, D. Kim, S. Jung and Y. Hwu, *Mater. Chem. Phys.*, 2011, **131**, 331–335.
68 Y. Yang, Y. Hu, X. Xiong and Y. Qin, *RSC Adv.*, 2013, **3**, 8431–8436.
69 R. Al-Gaashani, S. Radiman, N. Tabet and A. R. Daud, *Mater. Chem. Phys.*, 2011, **125**, 846–852.
70 W. Promnopas, T. Thongtem and S. Thongtem, *Superlattices Microstruct.*, 2015, **78**, 71–78.
71 M. Hasanpoor, M. Aliofkhazraei and H. Delavari, *Procedia Mater. Sci.*, 2015, **11**, 320–325.
72 B. Ashley, C. M. Dyer, J. Owens and G. F. Strouse, *J. Phys. Chem. C*, 2018, **122**, 3617–3627.
73 S. Horikoshi, H. Abe, T. Sumi, K. Torigoe, H. Sakai, N. Serpone and M. Abe, *Nanoscale*, 2011, **3**, 1697–1702.

74 S. Horikoshi, F. Sakai, M. Kajitani, M. Abe and N. Serpone, *Chem. Phys. Lett.*, 2009, **470**, 304–307.
75 E. K. Nyutu, C.-H. Chen, P. K. Dutta and S. L. Suib, *J. Phys. Chem. C*, 2008, **112**, 9659–9667.
76 E. Caponetti, L. Pedone and R. Massa, *Mater. Res. Innovations*, 2004, **8**, 44–47.
77 S. Riaz, R. Ashraf, A. Akbar and S. Naseem, *IEEE Trans. Magn.*, 2014, **50**, 1–4.
78 N. F. Jaafar, A. A. Jalil, S. Triwahyono and N. Shamsuddin, *RSC Adv.*, 2015, **5**, 90991–91000.
79 G. P. Barreto, G. Morales and M. L. L. Quintanilla, *J. Mater.*, 2013, **2013**, 478681.
80 B. L. Devi, K. M. Rao and D. Ramananda, *Inorg. Chem. Commun.*, 2022, **140**, 109460.
81 I. G. Shitu, J. Y. C. Liew, Z. A. Talib, H. Baqiah, M. M. A. Kechik, M. A. Kamarudin, N. H. Osman, Y. J. Low and I. I. Lakin, *ACS Omega*, 2021, **6**, 10698–10708.
82 P. E. Saloga, C. Kästner and A. F. Thünemann, *Langmuir*, 2018, **34**, 147–153.
83 S. Kazemzadeh, A. Hassanjani-Roshan, M. Vaezi and A. Shokuhfar, *Trans. Indian Inst. Met.*, 2011, **64**, 261–264.
84 J. W. Doolittle and P. K. Dutta, *Langmuir*, 2006, **22**, 4825–4831.
85 S. Al Azzam, Z. Ullah, S. Azmi, M. Islam, I. Ahmad and M. K. Hussain, *Beni-Suef Univ. J. Basic Appl. Sci.*, 2024, **13**, 53.
86 M. Maharaz, M. Halimah, S. Paiman, N. Saiden and I. Alibe, *Int. J. Electrochem. Sci.*, 2018, **13**, 9317–9332.
87 V. Polshettiwar, B. Baruwati and R. S. Varma, *ACS Nano*, 2009, **3**, 728–736.
88 T. Takai, A. Shibatani, Y. Asakuma, A. Saptoro and C. Phan, *Chem. Eng. Res. Des.*, 2022, **182**, 714–718.
89 D. M. Smith, J. K. Simon and J. R. Baker Jr, *Nat. Rev. Immunol.*, 2013, **13**, 592–605.
90 W. Ma, Y. Zhan, Y. Zhang, C. Mao, X. Xie and Y. Lin, *Signal Transduction Targeted Ther.*, 2021, **6**, 351.
91 L. Wei, J. Liu and G. Jiang, *Nat. Commun.*, 2024, **15**, 7389.
92 L. Wang, M. H. Kafshgari and M. Meunier, *Adv. Funct. Mater.*, 2020, **30**, 2005400.
93 Nanomaterials, https://ec.europa.eu/health/scientific_committees/opinions_layman/nanomaterials2012/de/index.htm#2.
94 W. Park, H. Shin, B. Choi, W.-K. Rhim, K. Na and D. K. Han, *Prog. Mater. Sci.*, 2020, **114**, 100686.
95 B. H. Alshammari, M. M. A. Lashin, M. A. Mahmood, F. S. Al-Mubaddel, N. Ilyas, N. Rahman, M. Sohail, A. Khan, S. S. Abdullaev and R. Khan, *RSC Adv.*, 2023, **13**, 13735–13785.
96 Y. Khan, H. Sadia, S. Z. A. Shah, M. N. Khan, A. A. Shah, N. Ullah, M. F. Ullah, H. Bibi, O. T. Bafakeeh and N. B. Khedher, *Catalysts*, 2022, **12**, 1386.
97 B. Mekuye and B. Abera, *Nano Sel.*, 2023, **4**, 486–501.
98 S. Yokoyama, A. Otomo, T. Nakahama, Y. Okuno and S. Mashiko, *Top. Curr. Chem.*, 2003, **228**, 205–226.
99 T. Fernandes, A. L. Daniel-da-Silva and T. Trindade, *Coord. Chem. Rev.*, 2022, **460**, 214483.
100 K. S. Soni, S. S. Desale and T. K. Bronich, *J. Controlled Release*, 2016, **240**, 109–126.
101 A. Zielińska, F. Carreiró, A. M. Oliveira, A. Neves, B. Pires, D. N. Venkatesh, A. Durazzo, M. Lucarini, P. Eder, A. M. Silva, A. Santini and E. B. Souto, *Molecules*, 2020, **25**, 3731.
102 M. J. Mitchell, M. M. Billingsley, R. M. Haley, M. E. Wechsler, N. A. Peppas and R. Langer, *Nat. Rev. Drug Discovery*, 2021, **20**, 101–124.
103 S. S. Guterres, M. P. Alves and A. R. Pohlmann, *Drug Target Insights*, 2007, **2**, 147–157.
104 F. Mascarenhas-Melo, A. Mathur, S. Murugappan, A. Sharma, K. Tanwar, K. Dua, S. K. Singh, P. G. Mazzola, D. N. Yadav, A. K. Rengan, F. Veiga and A. C. Paiva-Santos, *Eur. J. Pharm. Biopharm.*, 2023, **192**, 25–40.
105 M. Le Goas, J. Saber, S. G. Bolívar, J.-M. Rabanel, J.-M. Awogni, D. C. Boffito and X. Banquy, *Nano Today*, 2022, **45**, 101516.
106 J. Y. Oh, G. Yang, E. Choi and J.-H. Ryu, *Biomater. Sci.*, 2022, **10**, 1448–1455.
107 Y. Yu, A. Wang, S. Wang, Y. Sun, L. Chu, L. Zhou, X. Yang, X. Liu, C. Sha, K. Sun and L. Xu, *Mol. Pharm.*, 2022, **19**, 1219–1229.
108 A. Sood, A. Dev, M. N. Sardoiwala, S. R. Choudhury, S. Chaturvedi, A. K. Mishra and S. Karmakar, *Mater. Sci. Eng., C*, 2021, **129**, 112394.
109 V. Arora, A. Sood, J. Shah, R. K. Kotnala and T. K. Jain, *Mater. Sci. Eng., C*, 2017, **80**, 243–251.
110 O. V. Dement'eva and M. E. Kartseva, *Colloid J.*, 2023, **85**, 500–519.
111 H. Le-The, E. Berenschot, R. M. Tiggelaar, N. R. Tas, A. van den Berg and J. C. T. Eijkel, *Microsyst. Nanoeng.*, 2018, **4**, 4.
112 R. R. Arvizo, S. Bhattacharyya, R. A. Kudgus, K. Giri, R. Bhattacharya and P. Mukherjee, *Chem. Soc. Rev.*, 2012, **41**, 2943–2970.
113 J. Azadmanjiri, P. Kumar, V. K. Srivastava and Z. Sofer, *ACS Appl. Nano Mater.*, 2020, **3**, 3116–3143.
114 M. P. Nikolova and M. S. Chavali, *Biomimetics*, 2020, **5**, 27.
115 J. Kolosnjaj-Tabi, Y. Javed, L. Lartigue, J. Volatron, D. Elgrabli, I. Marangon, G. Pugliese, B. Caron, A. Figuerola, N. Luciani, T. Pellegrino, D. Alloyeau and F. Gazeau, *ACS Nano*, 2015, **9**, 7925–7939.
116 A. Shah and M. A. Dobrovolskaia, *Nanomedicine*, 2018, **14**, 977–990.
117 C. Pechyen, B. Tangnorawich, S. Toommee, R. Marks and Y. Parcharoen, *Sens. Int.*, 2024, **5**, 100287.
118 H. Chang, B. H. Kim, S. G. Lim, H. Baek, J. Park and T. Hyeon, *Inorg. Chem.*, 2021, **60**, 4261–4268.
119 G. Habibullah, J. Viktorova and T. Ruml, *Nanoscale Res. Lett.*, 2021, **16**, 47.
120 A. Sood, V. Arora, S. Kumari, A. Sarkar, S. S. Kumaran, S. Chaturvedi, T. K. Jain and G. Agrawal, *Int. J. Biol. Macromol.*, 2021, **189**, 443–454.

121 U. Kadiyala, N. A. Kotov and J. S. VanEpps, *Curr. Pharm. Des.*, 2018, **24**, 896–903.
122 S. Zhang, L. Lin, X. Huang, Y.-G. Lu, D.-L. Zheng and Y. Feng, *J. Nanomater.*, 2022, **2022**, 2063265.
123 A. Saka, S. R. Dey, L. T. Jule, R. Krishnaraj, R. Dhanabal, N. Mishra and N. Nagaprasad, *Sci. Rep.*, 2024, **14**, 26850.
124 D. Dharmaraj, M. Krishnamoorthy, K. Rajendran, K. Karuppiah, J. Annamalai, K. R. Durairaj, P. Santhiyagu and K. Ethiraj, *J. Drug Delivery Sci. Technol.*, 2021, **61**, 102111.
125 S. Gevorgyan, R. Schubert, S. Falke, K. Lorenzen, K. Trchounian and C. Betzel, *Sci. Rep.*, 2022, **12**, 14077.
126 A. Azam, A. S. Ahmed, M. Oves, M. S. Khan, S. S. Habib and A. Memic, *Int. J. Nanomed.*, 2012, **7**, 6003–6009.
127 A. M. El-Khawaga, A. Zidan and A. I. A. A. El-Mageed, *J. Mol. Struct.*, 2023, **1281**, 135148.
128 M. Roy, A. Roy, S. Rustagi and N. Pandey, *BioMed Res. Int.*, 2023, **2023**, 4838043.
129 K. Yang, L. Feng, X. Shi and Z. Liu, *Chem. Soc. Rev.*, 2013, **42**, 530–547.
130 A. Kalluri, B. Dharmadhikari, D. Debnath, P. Patra and C. V. Kumar, *ACS Omega*, 2023, **8**, 21358–21376.
131 V. Georgakilas, J. A. Perman, J. Tucek and R. Zboril, *Chem. Rev.*, 2015, **115**, 4744–4822.
132 H. Ashraf, T. Anjum, S. Riaz and S. Naseem, *Front. Microbiol.*, 2020, **11**, 238.
133 F. Maryani and A. W. Septama, *Mater. Adv.*, 2022, **3**, 8267–8275.
134 K. Devasvaran, B. Alallam, M. A. Yunus, F. R. P. Dewi, N. N. S. N. M. Kamal and V. Lim, *J. Drug Delivery Sci. Technol.*, 2023, **86**, 104688.
135 I. Jahan, F. Erci and I. Isildak, *Anal. Lett.*, 2019, **52**, 1860–1873.
136 R. P. I. Tormena, E. V. Rosa, B. F. O. Mota, J. A. Chaker, C. W. Fagg, D. O. Freire, P. M. Martins, I. C. Rodrigues da Silva and M. H. Sousa, *RSC Adv.*, 2020, **10**, 20676–20681.
137 F. Ulusu and Y. Ulusu, *Biol. Bull.*, 2024, **51**, 845–856.
138 A. P. Ajaykumar, O. Sabira, V. S. Binitha, S. R. Varma, A. Mathew, K. N. Jayaraj, P. A. Janish, K. V. Zeena, P. Sheena, V. Venugopal, P. Palakkapparambil and Aswathi, *Pharmaceutics*, 2023, **15**, 2468.
139 M. Aykur, N. G. Tosun, Ö. Kaplan and A. Özgür, *J. Drug Delivery Sci. Technol.*, 2023, **89**, 105013.
140 L. B. Anigol, V. P. Sajjan, P. M. Gurubasavaraj, S. V. Ganachari and D. Patil, *Chem. Pap.*, 2023, **77**, 3327–3345.
141 T. J. Mpala, M. H. Serepa-Dlamini, A. Etale, H. Richards and L. N. Nthunya, *Mater. Today Commun.*, 2023, **34**, 105028.
142 J. Pekkoh, K. Ruangrit, T. Kaewkod, Y. Tragoolpua, S. Hoijang, L. Srisombat, A. Wichapein, W. Pathom-aree, Y. Kato, G. Wang and S. Srinuanpan, *Nanomaterials*, 2023, **13**, 2141.
143 D. Pletzer, J. Asnis, Y. N. Slavin, R. E. W. Hancock, H. Bach, K. Saatchi and U. O. Häfeli, *Int. J. Pharm.*, 2021, **596**, 120299.
144 K. Moorthy, K.-C. Chang, H.-C. Huang, W.-J. Wu and C.-K. Chiang, *Antioxidants*, 2024, **13**, 32.
145 R. Vijayan, S. Joseph and B. Mathew, *Bionanoscience*, 2018, **8**, 105–117.
146 F. M. Aldakheel, D. Mohsen, M. M. El Sayed, K. A. Alawam, A. S. Binshaya and S. A. Alduraywish, *Molecules*, 2023, **28**, 3241.
147 M. Adnan, K. K. Oh, A. Husen, M. H. Wang, M. Alle and D. H. Cho, *Pharmaceuticals*, 2022, **15**, 111.
148 M. Shakibaie, R. Torabi-Shamsabad, H. Forootanfar, P. Amiri-Moghadam, B. Amirheidari, M. Adeli-Sardou and A. Ameri, *3 Biotech*, 2021, **11**, 511.
149 R. I. Priyadharshini, G. Prasannaraj, N. Geetha and P. Venkatachalam, *Appl. Biochem. Biotechnol.*, 2014, **174**, 2777–2790.
150 Ö. Kaplan, N. G. Tosun, A. Özgür, S. E. Tayhan, S. Bilgin, İ. Türkekul and İ. Gökce, *J. Drug Delivery Sci. Technol.*, 2021, **64**, 102641.
151 K. Seku, B. Pejjai, A. I. Osman, S. S. Hussaini, M. Al-Abri, R. Swathi, M. Hussain, N. S. Kumar, A. S. Al-Fatesh and G. B. Reddy, *J. Colloid Interface Sci.*, 2024, **659**, 718–727.
152 I. Jahan, F. Erci and I. Isildak, *J. Drug Delivery Sci. Technol.*, 2021, **61**, 102172.
153 N. Sreeju, A. Rufus and D. Philip, *J. Mol. Liq.*, 2016, **221**, 1008–1021.
154 R. E. Nimshi, J. J. Vijaya, M. Bououdina, L. J. Kennedy, B. Al-Najar and O. Lemine, *J. Inorg. Organomet. Polym. Mater.*, 2023, **33**, 1016–1027.
155 M. Shakibaie, S. Riahi-Madvar, A. Ameri, P. Amiri-Moghadam, M. Adeli-Sardou and H. Forootanfar, *J. Cluster Sci.*, 2022, **33**, 1877–1887.
156 M. Shakibaie, H. Forootanfar, E. Jafari, A. Salimi, M. Doostmohammadi and H.-R. Rahimi, *Toxicol. Environ. Chem.*, 2020, **102**, 386–398.
157 S. Azizi, R. Mohamad and M. M. Shahri, *Molecules*, 2017, **22**, 301.
158 A. Salimi, R. Hamid-Reza, F. Hamid, J. Elham, A. Atefeh and M. Shakibaie, *Artif. Cells, Nanomed., Biotechnol.*, 2019, **47**, 1846–1858.
159 Abisha Meji M, Usha D and Ashwin B M, *Mater. Res. Express*, 2024, **11**, 085004.
160 W. Li, Q. You, J. Zhang, W. Li and H. Xu, *J. Alloys Compd.*, 2023, **947**, 169697.
161 A. Ameri, M. Shakibaie, H. R. Rahimi, M. Adeli-Sardou, M. Raeisi, A. Najafi and H. Forootanfar, *Biol. Trace Elem. Res.*, 2020, **197**, 132–140.
162 H. M. Alkhalidi, U. Zaman, D. Khan, K. ur Rehman, K. I. Omar, M. Alissa, W. Y. Rizg, D. M. Bukhary, E. A. Abdelrahman, M. S. Refat, A. M. Alsuhaibani and H. Fetooh, *J. Mol. Liq.*, 2023, **392**, 123469.
163 V. Jeevanantham, D. Tamilselvi, K. Rathidevi and S. R. Bavaji, *J. Mater. Res.*, 2023, **38**, 1909–1918.
164 N. S. Zidan, N. M. Abdulsalam, N. A. Khateeb, M. A. Hijazi, A. A. Alrasheedi, G. ElMasry, S. Al-Rejaie, G. M. Al-Jahani and A. I. Alalawy, *J. Mol. Struct.*, 2024, **1295**, 136715.

165 C. Mellinas, A. Jiménez and M. d. C. Garrigós, *Molecules*, 2019, **24**, 4048.
166 N. Satarzadeh, M. Shakibaie, M. Adeli-Sardou, F. Jabari-Morouei, H. Forootanfar and A. Sadeghi-Dousari, *J. Cluster Sci.*, 2023, **34**, 1831–1839.
167 Y. Wu, W. Chen, J. Deng, X. Cao, Z. Yang, J. Chen, Q. Tan, E. Zhou, M. Li, J. Liu, M. Guo and Y. Jin, *Nat. Nanotechnol.*, 2025, **20**, 1119–1130.
168 A. Gebril, M. A. Obeid, E. M. Bennett, A. Pujol, M. L. Chovel, T. Mahy, R. Acevedo and V. A. Ferro, *Eur. J. Pharm. Biopharm.*, 2022, **171**, 11–18.
169 S. S. Dunn, D. R. B. Vera, S. R. Benhabbour and M. C. Parrott, *J. Colloid Interface Sci.*, 2017, **488**, 240–245.
170 N. Garino, T. Limongi, B. Dumontel, M. Canta, L. Racca, M. Laurenti, M. Castellino, A. Casu, A. Falqui and V. Cauda, *Nanomaterials*, 2019, **9**, 212.
171 M. Masjedi-Arani, M. Amiri, O. Amiri, M. Ahmadi and M. Salavati-Niasari, *Int. J. Pharm.*, 2020, **591**, 120021.
172 B. Srinivasan, E. Kolanthai, E. A. K. Nivethaa, M. S. Pandian, P. Ramasamy, L. H. Catalani and S. N. Kalkura, *Ceram. Int.*, 2023, **49**, 855–861.
173 M. Kheradmandfard, S. F. Kashani-Bozorg, M. R. Barati and S. Sarfarazijami, *J. Mater. Res. Technol.*, 2023, **25**, 1735–1747.
174 M. Kheradmandfard, S. F. Kashani-Bozorg, A. H. Noori-Alfesharaki, A. Z. Kharazi, M. Kheradmandfard and N. Abutalebi, *Mater. Sci. Eng., C*, 2018, **92**, 236–244.
175 C. Qi, Y.-J. Zhu and F. Chen, *ACS Appl. Mater. Interfaces*, 2014, **6**, 4310–4320.
176 X.-Y. Zhao, Y.-J. Zhu, F. Chen, B.-Q. Lu and J. Wu, *CrystEngComm*, 2013, **15**, 206–212.
177 K. Seku, B. Pejjai, A. I. Osman, S. S. Hussaini, M. Al-Abri, R. Swathi, M. Hussain, N. S. Kumar, A. S. Al-Fatesh and G. Bhagavanth Reddy, *J. Colloid Interface Sci.*, 2024, **659**, 718–727.
178 H. Hassan, N. K. Sedky, M. S. Nafie, N. K. Mahdy, I. M. Fawzy, T. W. Fayed, E. Preis, U. Bakowsky and S. A. Fahmy, *Molecules*, 2024, **29**, 5327.
179 A. S. Alhawiti, *Biomass Convers. Biorefin.*, 2024, **14**, 6581–6590.
180 R. P. Illanes Tormena, M.-K. Medeiros Salviano Santos, A. Oliveira da Silva, F. M. Félix, J. A. Chaker, D. O. Freire, I. C. Rodrigues da Silva, S. E. Moya and M. H. Sousa, *RSC Adv.*, 2024, **14**, 22035–22043.
181 K. Devasvaran, B. Alallam, C. Lee, Y. K. Yong and V. Lim, *Int. J. Biol. Macromol.*, 2024, **278**, 134893.
182 S. S. Murugan, P. A. Dalavi, P. K. Gupta, W. Hur, R. Pillappan, J. Venkatesan and G. H. Seong, *Adv. Nat. Sci.: Nanosci. Nanotechnol.*, 2024, **15**, 045002.
183 M. A. A. Fayed, I. A. Abdallah, I. Ahmad, H. Patel and E. M. Abdou, *J. Mol. Struct.*, 2024, **1314**, 138800.
184 I. R. S. Vieira, A. A. da Silva, B. D. da Silva, L. T. Neto, L. Tessaro, A. K. O. Lima, M. P. Garcia, J. A. d. A. Ribeiro, C. M. Rodrigues, A. M. F. de Sousa, N. M. F. Carvalho, A. Rajkovic and C. A. Conte-Junior, *Waste Biomass Valorization*, 2024, **15**, 4717–4734.
185 N. K. Sedky, I. M. Fawzy, A. Hassan, N. K. Mahdy, R. T. Attia, S. N. Shamma, M. Y. Alfaifi, S. E. Elbehairi, F. A. Mokhtar and S. A. Fahmy, *RSC Adv.*, 2024, **14**, 4005–4024.
186 T. V. de Medeiros, J. Manioudakis, F. Noun, J.-R. Macairan, F. Victoria and R. Naccache, *J. Mater. Chem. C*, 2019, **7**, 7175–7195.
187 C. O. Kappe, *Angew. Chem., Int. Ed.*, 2004, **43**, 6250–6284.
188 A. Sosnik, G. Gotelli and G. A. Abraham, *Prog. Polym. Sci.*, 2011, **36**, 1050–1078.
189 M. Baghbanzadeh, L. Carbone, P. D. Cozzoli and C. O. Kappe, *Angew. Chem., Int. Ed.*, 2011, **50**, 11312–11359.
190 C. Gabriel, S. Gabriel, E. H. Grant, E. H. Grant, B. S. J. Halstead, D. Michael and P. Mingos, *Chem. Soc. Rev.*, 1998, **27**, 213–224.
191 N. Soltani, E. Saion, M. Erfani, K. Rezaee, G. Bahmanrokh, G. P. Drummen, A. Bahrami and M. Z. Hussein, *Int. J. Mol. Sci.*, 2012, **13**, 12412–12427.
192 F. Fievet, J. P. Lagier, B. Blin, B. Beaudoin and M. Figlarz, *Solid State Ionics*, 1989, **32–33**, 198–205.
193 Z. Ma, J. Yu and S. Dai, *Adv. Mater.*, 2010, **22**, 261–285.
194 N. E. Leadbeater and H. M. Torenius, *J. Org. Chem.*, 2002, **67**, 3145–3148.
195 D. Obermayer and C. O. Kappe, *Org. Biomol. Chem.*, 2010, **8**, 114–121.
196 R. G. Compton, B. A. Coles and F. Marken, *Chem. Commun.*, 1998, 2595–2596, DOI: 10.1039/A806511J.
197 K. Soliwoda, E. Tomaszewska, B. Tkacz-Szczesna, E. Mackiewicz, M. Rosowski, A. Bald, C. Blanck, M. Schmutz, J. Novák, F. Schreiber, G. Celichowski and J. Grobelny, *Langmuir*, 2014, **30**, 6684–6693.
198 Z. Liu, X. Y. Ling, X. Su and J. Y. Lee, *J. Phys. Chem. B*, 2004, **108**, 8234–8240.
199 J.-S. Xu and Y.-J. Zhu, *Mater. Lett.*, 2011, **65**, 2793–2796.
200 S. K. Apte, S. D. Naik, R. S. Sonawane, B. B. Kale, N. Pavaskar, A. B. Mandale and B. K. Das, *Mater. Res. Bull.*, 2006, **41**, 647–654.
201 N. Mir and M. Salavati-Niasari, *Mater. Res. Bull.*, 2013, **48**, 1660–1667.
202 S. Gyergyek, D. Makovec and M. Drofenik, *J. Colloid Interface Sci.*, 2011, **354**, 498–505.
203 M. Panahi-Kalamuei, M. Salavati-Niasari and S. M. Hosseinpour-Mashkani, *J. Alloys Compd.*, 2014, **617**, 627–632.
204 T. Zhang, T. Doert, K. Schwedtmann, J. J. Weigand and M. Ruck, *Dalton Trans.*, 2020, **49**, 1891–1896.
205 P. J. Goulet, G. R. Bourret and R. B. Lennox, *Langmuir*, 2012, **28**, 2909–2913.
206 F. J. Douglas, D. A. MacLaren and M. Murrie, *RSC Adv.*, 2012, **2**, 8027–8035.
207 V. J. Law and D. P. Dowling, *Am. J. Anal. Chem.*, 2023, **14**, 149–174.
208 K. ur Rehman, K. M. Albalawi, S. Badshah, M. Alissa, S. A. Alghamdi, A. Alghamdi, M. A. Alshehri, G. S. Aloraini, M. Essid and E. A. Abdelrahman, *J. Taiwan Inst. Chem. Eng.*, 2025, **170**, 106004.

209 A. Roy and K. Manna, in *Biomass-Based Functional Carbon Nanostructures for Supercapacitors*, ed. S. K. Tiwari, M. Bystrzejewski and V. Kumar, Springer Nature Singapore, Singapore, 2023, pp. 41–74. DOI: 10.1007/978-981-99-0996-4_2.
210 A. Roy and C. K. Maity, in *Advanced Applications of 2D Nanostructures: Emerging Research and Opportunities*, ed. S. Singh, K. Verma and C. Prakash, Springer Singapore, Singapore, 2021, pp. 211–229. DOI: 10.1007/978-981-16-3322-5_11.
211 V. Harish, M. M. Ansari, D. Tewari, A. B. Yadav, N. Sharma, S. Bawarig, M.-L. García-Betancourt, A. Karatutlu, M. Bechelany and A. Barhoum, *J. Taiwan Inst. Chem. Eng.*, 2023, **149**, 105010.
212 S. K. J. Arunpandian Balaji, E. Supriyanto, I. I. Muhamad and A. Z. Md Khudzari, *Int. J. Nanomed.*, 2015, **10**, 5909–5923.
213 N. Verma, D. Pathak, K. Kumar, K. Jeet, S. Nimesh, L. Loveleen, S. Kumar and N. Thakur, *Mater. Chem. Phys.*, 2025, **333**, 130422.
214 F. Du, J. Niu, Y. Hong, X. Fang, Z. Geng, J. Liu, F. Xu, T. Liu, Q. Chen and J. Zhai, *Int. J. Nanomed.*, 2025, 523–540.
215 Y. Venkatesh, P. V. S. Naidu, M. Ramanjaneyulu, P. A. Rao and D. B. Kundrapu, *J. Nanopart. Res.*, 2025, **27**, 62.
216 M. F. M. Yusoff, N. H. A. Kasim, W. H. Himratul-Aznita, S. Saidin, K. Genasan, T. Kamarul and Z. Radzi, *Mater. Charact.*, 2021, **178**, 111169.
217 K. R. Ahammed, M. Ashaduzzaman, S. C. Paul, M. R. Nath, S. Bhowmik, O. Saha, M. M. Rahaman, S. Bhowmik and T. D. Aka, *SN Appl. Sci.*, 2020, **2**, 955.
218 B. Ashwin, A. Yardily and M. S. Dennison, *Discover Appl. Sci.*, 2025, **7**, 177.
219 M. Kheradmandfard, K. Mahdavi, A. Z. Kharazi, S. F. Kashani-Bozorg and D.-E. Kim, *Mater. Sci. Eng., C*, 2020, **117**, 111310.
220 S. Mondal, G. Hoang, P. Manivasagan, M. S. Moorthy, T. T. Vy Phan, H. H. Kim, T. P. Nguyen and J. Oh, *Ceram. Int.*, 2019, **45**, 2977–2988.
221 M. Irfan, A. Jeshurun and B. M. Reddy, *Dalton Trans.*, 2025, **54**, 3774–3795.
222 A. Roy, S. Samanta, K. Singha, P. Maity, N. Kumari, A. Ghosh, S. Dhara and S. Pal, *ACS Appl. Bio Mater.*, 2020, **3**, 3285–3293.
223 W. Chen, Y. Zhong, G. Fu, W. Lai, Z. Pan, Y. Yang, F. Chen and H. Yan, *Coatings*, 2023, **13**, 31.
224 G. Karunakaran, E.-B. Cho, G. S. Kumar, E. Kolesnikov, A. Dmitry and S. Ali, *Ceram. Int.*, 2021, **47**, 8642–8652.
225 A.-C. Burdusel, I. A. Neacsu, A. C. Birca, C. Chircov, A.-M. Grumezescu, A. M. Holban, C. Curutiu, L. M. Ditu, M. Stan and E. Andronescu, *J. Funct. Biomater.*, 2023, **14**, 378.
226 S. Kar, T. Kaur and A. Thirugnanam, *Int. J. Biol. Macromol.*, 2016, **82**, 628–636.
227 M. P. Romero, F. Alves, M. D. Stringasci, H. H. Buzzá, H. Ciol, N. M. Inada and V. S. Bagnato, *Front. Microbiol.*, 2021, **12**, 662149.
228 X. Jiang, Z. Luo, B. Zhang, P. Li, J. a. Xiao and W. Su, *Inorg. Chem. Commun.*, 2022, **142**, 109543.
229 K. Dechsri, C. Suwanchawalit, P. Patrojanasophon, P. Opanasopit, S. Pengnam, T. Charoenying and T. Taesotikul, *Pharmaceutics*, 2024, **16**, 254.
230 M. Kheradmandfard, F. Nejatidanesh, O. Savabi and D.-E. Kim, *Inorg. Chem. Commun.*, 2025, 114749.
231 C. K. Thakur, C. Karthikeyan, M. S. Abou-Dahech, M. M. A. M. Altabakha, M. J. S. Al Shahwan, C. R. Ashby, A. K. Tiwari, R. J. Babu and N. S. H. N. Moorthy, *Pharmaceutics*, 2023, **15**, 335.
232 D. K. Becerra-Paniagua, E. B. Díaz-Cruz, A. Baray-Calderón, A. R. Garcia-Angelmo, E. Regalado-Pérez, M. del Pilar Rodriguez-Torres and C. Martínez-Alonso, *J. Mater. Sci.: Mater. Electron.*, 2022, **33**, 22631–22667.
233 Y. Xie, T. Liu, Z. Chu and W. Jin, *J. Electroanal. Chem.*, 2021, **893**, 115328.
234 A. Tripathy, M. J. Nine and F. S. Silva, *Adv. Colloid Interface Sci.*, 2021, **290**, 102380.
235 Z. Ye, W. Liao, Z. Deng, L. Wang, B. Wen, D. Zhang, H. Wang, W. Xie and H. Peng, *TrAC, Trends Anal. Chem.*, 2024, **175**, 117724.
236 S. S. Rao, K. Saptami, J. Venkatesan and P. D. Rekha, *Int. J. Biol. Macromol.*, 2020, **163**, 745–755.
237 W. Alghazzawi, E. Danish, H. Alnahdi and M. A. Salam, *Synth. Met.*, 2020, **267**, 116401.
238 Q. Bu, J. Cai, S. V. Vasudevan, J. Ni and H. Mao, *Electrochim. Acta*, 2021, **398**, 139319.
239 S. Rafique, M. B. Sadiq, R. Akram, M. Hussain, M. Rizwan, M. Bashir, J. S. Khan and S. U. Awan, *J. Mater. Res.*, 2023, **38**, 2401–2412.
240 K. Pei, D. Li, W. Qi and D. Wu, *Molecules*, 2023, **28**, 1892.
241 X. Li, H. Dong, Q. Fan, K. Chen, D. Sun, T. Hu and Z. Ni, *Microchem. J.*, 2022, **179**, 107468.
242 F. Hekmat, M. Ezzati, S. Shahrokhian and H. E. Unalan, *J. Electroanal. Chem.*, 2021, **890**, 115244.
243 A. D. Savariraj, V. Vinoth, R. V. Mangalaraja, T. Arun, D. Contreras, A. Akbari-Fakhrabadi, H. Valdés and F. Banat, *J. Electroanal. Chem.*, 2020, **856**, 113629.
244 L. Kennedy, J. K. Sandhu, M.-E. Harper and M. Cuperlovic-Culf, *Biomolecules*, 2020, **10**, 1429.
245 K. Makris, C. Mousa and E. Cavalier, *Calcif. Tissue Int.*, 2023, **112**, 233–242.
246 C.-L. Sun, C.-T. Chang, H.-H. Lee, J. Zhou, J. Wang, T.-K. Sham and W.-F. Pong, *ACS Nano*, 2011, **5**, 7788–7795.
247 T. Maity, S. Jain, M. Solra, S. Barman and S. Rana, *ACS Sustainable Chem. Eng.*, 2022, **10**, 1398–1407.
248 A. Taneja, P. Gupta, S. Thatai, P. Khurana, K. R. Ranjan, J. Singh and M. D. Mukherjee, *J. Mol. Struct.*, 2024, **1318**, 139320.
249 T. Girardet, E. Bianchi, C. Henrionnet, A. Pinzano, S. Bouguet-Bonnet, C. Boulogne, S. Leclerc, F. Cleymand and S. Fleutot, *Mater. Today Commun.*, 2023, **36**, 106819.
250 K. Hagiwara, S. Horikoshi and N. Serpone, *J. Photochem. Photobiol., A*, 2021, **415**, 113310.

251 R. De, K. W. Jo, B. H. Lee, S. Some and K.-T. Kim, *J. Mater. Chem. B*, 2023, **11**, 6024–6043.
252 N. Sharma, I. Sharma and M. K. Bera, *J. Fluoresc.*, 2022, **32**, 1039–1049.
253 N. Architha, M. Ragupathi, C. Shobana, T. Selvankumar, P. Kumar, Y. S. Lee and R. K. Selvan, *Environ. Res.*, 2021, **199**, 111263.
254 Y. Du, J. Zhou, F. He, P. Zang, H. Gong, C. Liu and P. Yang, *Nano Today*, 2023, **52**, 101963.
255 K. Perveen, F. M. Husain, F. A. Qais, A. Khan, S. Razak, T. Afsar, P. Alam, A. M. Almajwal and M. M. A. Abulmeaty, *Biomolecules*, 2021, **11**, 197.
256 K. Dechsri, C. Suwanchawalit, P. Chitropas, T. Ngawhirunpat, T. Rojanarata, P. Opanasopit and S. Pengnam, *AAPS PharmSciTech*, 2023, **24**, 135.
257 G. Murali, B. Kwon, H. Kang, J. K. R. Modigunta, S. Park, S. Lee, H. Lee, Y. H. Park, J. Kim and S. Y. Park, *ACS Appl. Nano Mater.*, 2022, **5**, 4376–4385.
258 M. J. Saadh, N. N. A. Jafar, F. M. A. Altalbawy, P. Sharma, A. Kumar, H. T. A. Alamir, H. Ghazy, M. Noori Shakir, S. K. Mohammed, K. Muzammil and B. Chasib Gabal, *RSC Adv.*, 2024, **14**, 24473–24482.
259 D. Zhi, T. Yang, J. O'Hagan, S. Zhang and R. F. Donnelly, *J. Controlled Release*, 2020, **325**, 52–71.
260 C. Zhang, H. Pan, X. Wang and S.-K. Sun, *Biomater. Sci.*, 2018, **6**, 2750–2756.
261 S. A. A. Vandarkuzhali, G. Karthikeyan and M. P. Pachamuthu, *J. Environ. Chem. Eng.*, 2021, **9**, 106411.
262 Y. Chen, M. Jiang, L. Xiong, X. Yao, M. Fan, D. Chen, Q. Jiang, Z. Jin and Q. He, *Chin. Chem. Lett.*, 2021, **32**, 3487–3490.
263 H. Liu, C. Xu, M. Meng, S. Li, S. Sheng, S. Zhang, W. Ni, H. Tian and Q. Wang, *Acta Biomater.*, 2022, **144**, 132–141.
264 Y. Jin, H. Qiao, Y. Zhang, Y. He, S. Xie, Y. Gu and F. Lin, *Carbon Lett.*, 2025, **35**, 813–823.
265 S. Tang, C. Peng, J. Xu, B. Du, Q. Wang, R. D. Vinluan III, M. Yu, M. J. Kim and J. Zheng, *Angew. Chem., Int. Ed.*, 2016, **55**, 16039–16043.
266 Z. Ye, W. Liao, Z. Deng, L. Wang, B. Wen, D. Zhang, H. Wang, W. Xie and H. Peng, *TrAC, Trends Anal. Chem.*, 2024, 117724.
267 N. Sohal, B. Maity and S. Basu, *ACS Appl. Bio Mater.*, 2021, **4**, 5158–5168.
268 Q. Bu, J. Cai, S. V. Vasudevan, J. Ni and H. Mao, *Electrochim. Acta*, 2021, **398**, 139319.
269 A. D. Savariraj, V. Vinoth, R. Mangalaraja, T. Arun, D. Contreras, A. Akbari-Fakhrabadi, H. Valdés and F. Banat, *J. Electroanal. Chem.*, 2020, **856**, 113629.
270 S. A. A. Vandarkuzhali, G. Karthikeyan and M. Pachamuthu, *J. Environ. Chem. Eng.*, 2021, **9**, 106411.
271 K. Kannan, D. Radhika, S. Vijayalakshmi, K. K. Sadasivuni, A. A. Ojiaku and U. Verma, *Int. J. Environ. Anal. Chem.*, 2022, **102**, 1095–1108.
272 D. Usha and B. Ashwin, *Mater. Res. Express*, 2024, **11**, 085004.
273 M. Kheradmandfard, K. Mahdavi, A. Z. Kharazi, S. F. Kashani-Bozorg and D.-E. Kim, *Mater. Sci. Eng., C*, 2020, **117**, 111310.
274 K. R. Ahammed, M. Ashaduzzaman, S. C. Paul, M. R. Nath, S. Bhowmik, O. Saha, M. M. Rahaman, S. Bhowmik and T. D. Aka, *SN Appl. Sci.*, 2020, **2**, 1–14.
275 S. Mondal, G. Hoang, P. Manivasagan, M. S. Moorthy, T. T. V. Phan, H. H. Kim, T. P. Nguyen and J. Oh, *Ceram. Int.*, 2019, **45**, 2977–2988.
276 A. Balaji, S. K. Jaganathan, E. Supriyanto, I. I. Muhamad and A. Z. M. Khudzari, *Int. J. Nanomed.*, 2015, 5909–5923.
277 C. K. Thakur, C. Karthikeyan, M. S. Abou-Dahech, M. M. A. Altabakha, M. J. S. Al Shahwan, C. R. Ashby Jr, A. K. Tiwari, R. J. Babu and N. S. H. N. Moorthy, *Pharmaceutics*, 2023, **15**, 335.
278 K. L. López, A. Ravasio, J. V. González-Aramundiz and F. C. Zacconi, *Pharmaceutics*, 2023, **15**, 1333.
279 A. Roy, R. Afshari, S. Jain, Y. Zheng, M.-H. Lin, S. Zenkar, J. Yin, J. Chen, N. A. Peppas and N. Annabi, *Chem. Soc. Rev.*, 2025, **54**, 2595–2652.
280 E. O. Aluko, A. S. Adekunle, J. A. Oyekunle and O. S. Oluwafemi, *J. Fluoresc.*, 2025, 1–27.
281 E. Mostafavi and H. Zare, *OpenNano*, 2022, **7**, 100062.
282 M. Shah, N. Shah, I. Shah, I. Shah, T. Rehan, K. Mammadova, A. Khan, N. Majeed, M. Anjum and M. Elodemi, *Results Eng.*, 2025, **26**, 104552.
283 M. Kheradmandfard, A. Sadeghian, M. Kouhi, Z. S. Sajadi-Javan, J. Varshosaz, O. Savabi and D.-E. Kim, *Surf. Interfaces*, 2025, 106626.
284 S. C. Hernández, L. Saludas-Echauri, M. J. Blanco-Prieto, P. Vader, A. Ruiz-Villalba, E. Garbayo and F. Prosper-Cardoso, *Eur. J. Pharm. Biopharm*, 2022, **170**, 187–196.